U.S.NRC
United States Nuclear Regulatory Commission
Protecting People and the Environment

RIL 2025-08

Implementation of Straight and Bend Pipe Elements in OpenSees

A Modern Replacement for PSAFE2 (a Legacy Code for Piping Analysis)

Date Published: September 2025

Prepared by:

M. Scott
M. Zhu

Developers of OpenSeesPy
Portwood Digital, LLC
Corvallis, OR 97330

Jinsuo Nie, NRC Project Manager

Research Information Letter
Office of Nuclear Regulatory Research

Disclaimer

Legally binding regulatory requirements are stated only in laws, NRC regulations, licenses, including technical specifications, or orders; not in Research Information Letters (RILs). A RIL is not regulatory guidance, although NRC's regulatory offices may consider the information in a RIL to determine whether any regulatory actions are warranted.

FORWORD

Research Information Letter 2025-08, "*Implementation of Straight and Bend Pipe Elements in OpenSees*," presents the formulation and implementation of straight and bend pipe elements that account for mechanical, pressure, and thermal load effects. These element formulations are available in the OpenSeesPy package (https://pypi.org/project/openseespy/), starting with version 3.7.0.4.

The implementation of these piping elements into OpenSees enhances the analytical capabilities of NRC staff in developing the technical bases for updating Regulatory Guide (RG) 1.92, "Combining Modal Responses and Spatial Components in Seismic Response Analysis," and RG 1.122, "Development of Floor Design Response Spectra for Seismic Design of Floor-Supported Equipment or Components." OpenSeesPy supports structural and mechanical engineers in conducting seismic analyses of structures, systems, and components.

This report and the associated code development were completed under a contract between the Office of Nuclear Regulatory Research, Division of Engineering, and Portwood Digital, LLC.

Implementation of Straight and Bend Pipe Elements in OpenSees

Michael H. Scott and Minjie Zhu

Prepared for Nuclear Regulatory Commission (NRC)

September 30, 2024

(Updated on October 30, 2024)

Abstract

The application of modal analysis, response spectra, and response history analysis to the design and assessment of nuclear power facilities requires the simulation of multiple structural and component models to several input loading histories, e.g., from ground motion records.

Outside of "ordinary" building structures, nuclear power facilities present challenging technical issues related to modal analysis, response spectrum analysis, and response history analysis for high frequency ground motions at sites in the Central and Eastern United States. Many of these issues stem from high frequency modes as well as closely spaced modes.

The PSAFE2 software (based largely on SAP-V) was developed for NRC by Brookhaven National Laboratory in the 1990s. PSAFE2 is a FORTRAN program (mostly pre-F77) that has become difficult to maintain and use with modern computing resources. However, PSAFE2 contains two piping elements (straight and bend) that are essential to accomplishing NRC goals and addressing technical issues related to the seismic assessment of nuclear power facilities.

OpenSees, the Open System for Earthquake Engineering Simulation [9, 7], and specifically, its Python module, OpenSeesPy [11], has become an essential tool for simulating static and dynamic response of the structural systems in nuclear power facilities. With its scripting capabilities, OpenSeesPy allows NRC engineers to examine structural response to multiple ground motion records and to quickly visualize results.

However, the two piping PSAFE2 elements are not available in OpenSees. As a result, extracting the piping elements from PSAFE2 and linking the elements with OpenSees will allow NRC staff to directly use these elements without having to develop more refined models from basic, pre-existing OpenSees elements, e.g., beam and shell elements.

This report describes the formulation and implementation of straight and bend pipe elements that include mechanical, pressure, and thermal load effects. The element formulations are available in the OpenSeesPy pip package (`https://pypi.org/project/openseespy/`) starting with version 3.7.0.4. Several verification examples are included with this report and the results of static and dynamic analyses of the BM3 benchmark pipe network model are presented. Analysis results with the newly formulated OpenSees pipe elements are shown to be very close to the results obtained with PSAFE2 (SAP-V).

Contents

List of Figures

List of Tables

Chapter 1

Formulation for 3D straight pipe element

The formulation for straight pipe elements follows standard theory for beam elements where the element response is formulated in basic, local, and global coordinate systems [4]. Additional details of the straight pipe element for internal pressure are based on [1] and accompanying SAP source code obtained from NISEE [8].

1.1 Global, local, and basic systems

The global DOFs for a straight pipe element in 3D is shown in Fig. 1.1. Degrees of freedom 1,2,3 (7,8,9) are translations along the global X,Y,Z axes and DOFs 4,5,6 (10,11,12) are rotations about the global axes at end I (J).

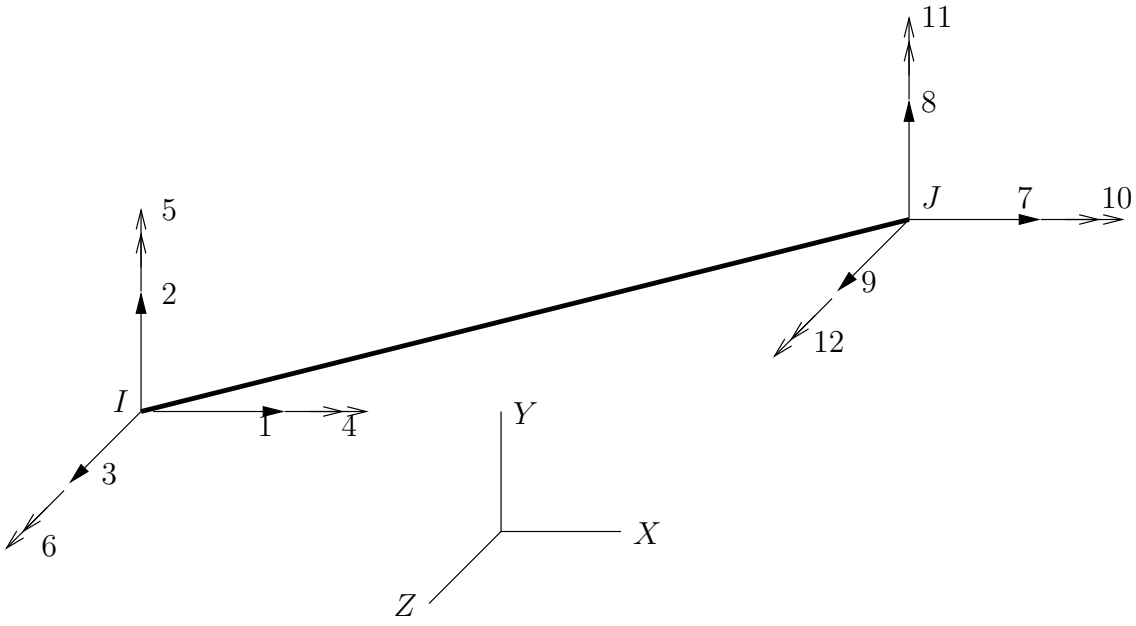

Figure 1.1: Global system for a straight pipe element in 3D.

Single headed arrows indicate translations while double headed arrows indicate rotations. The displacements (inclusive of translations and rotations) along or about each global DOF are collected in the vector $\mathbf{u} = [u_1 \dots u_{12}]^T$. while the corresponding forces and moments are collected in the vector $\mathbf{p} = [p_1 \dots p_{12}]^T$.

The local system for a straight pipe element coincides with the longitudinal axis, x, and two transverse axes, y and z, as shown in Fig.1.2.

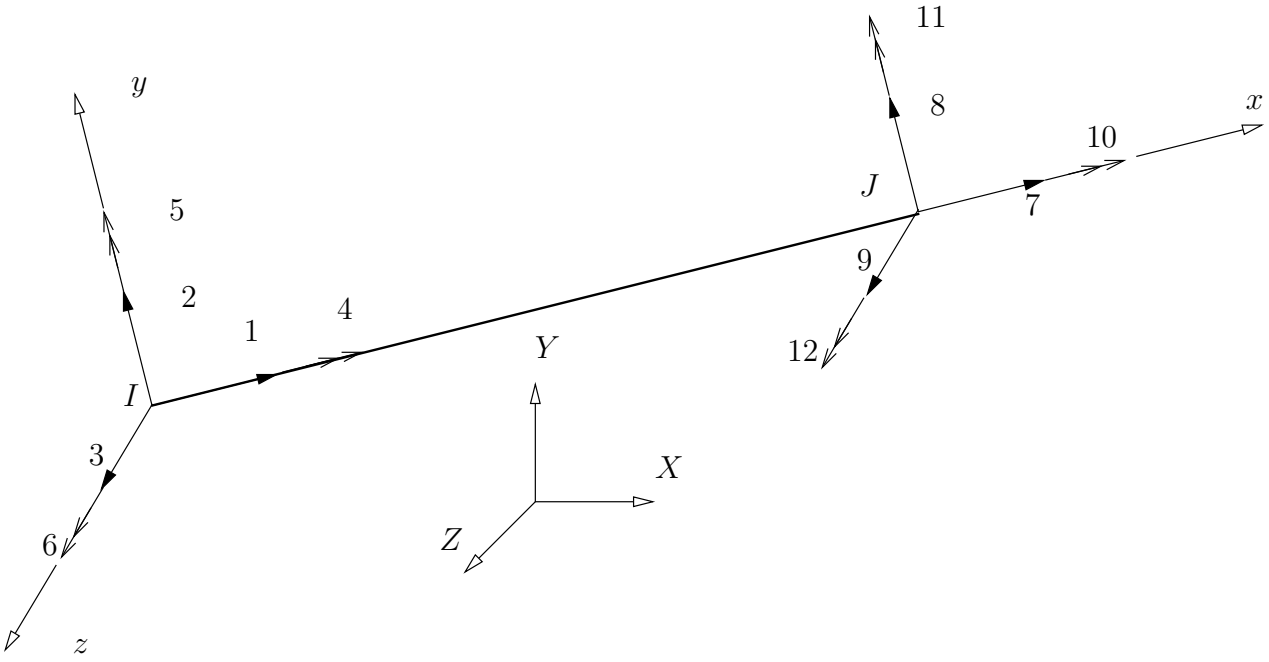

Figure 1.2: Local system for a straight pipe element in 3D.

The local x axis points from end I to end J while the local y and z axes are specified by the analyst. Similar to the global system, the DOFs in the local system are numbered 1,2,3 (7,8,9) for translations at I (J) and 4,5,6 (10,11,12) for rotations at I (J).

With the local axes known in three-dimensional space, $\mathbf{x} = [x_1, x_2, x_3]$, $\mathbf{y} = [y_1, y_2, y_3]$, and $\mathbf{z} = [z_1, z_2, z_3]$, the transformation of displacements and forces between the global and local system is described by the following matrix

$$\mathbf{a}_{lg} = \begin{bmatrix} x_1 & x_2 & x_3 & & & & & & & & & \\ y_1 & y_2 & y_3 & & & & & & & & & \\ z_1 & z_2 & z_3 & & & & & & & & & \\ & & & x_1 & x_2 & x_3 & & & & & & \\ & & & y_1 & y_2 & y_3 & & & & & & \\ & & & z_1 & z_2 & z_3 & & & & & & \\ & & & & & & x_1 & x_2 & x_3 & & & \\ & & & & & & y_1 & y_2 & y_3 & & & \\ & & & & & & z_1 & z_2 & z_3 & & & \\ & & & & & & & & & x_1 & x_2 & x_3 \\ & & & & & & & & & y_1 & y_2 & y_3 \\ & & & & & & & & & z_1 & z_2 & z_3 \end{bmatrix} \tag{1.1}$$

With this linear transformation matrix, we can transform displacements from the global to local system and, with the matrix transpose, forces from the local to global system:

$$\begin{aligned} \mathbf{u}_l &= \mathbf{a}_{lg}\mathbf{u} \\ \mathbf{p} &= \mathbf{a}_{lg}^T\mathbf{p}_l \end{aligned} \tag{1.2}$$

The element displacement field has six rigid body displacement modes within the local coordinate system. To deal with only the deformational modes and to easily incorporate loads effects due to pressure and thermal expansion, the element formulation drills down to a basic, or natural, system of six DOFs. Although several choices for basic system are possible, the pipe element is based on the simply-supported basic system where the deformations and corresponding forces correspond to the deformations and forces of a simply-supported beam.

The six basic forces are a subset of the local forces (axial force at end J, moments at I and J, and torsion at end J)

$$p_{b1} = p_{l7}, \quad p_{b4} = p_{l5} \tag{1.3}$$

$$p_{b2} = p_{l6}, \quad p_{b5} = p_{l11} \tag{1.4}$$

$$p_{b3} = p_{l12}, \quad p_{b6} = p_{l10} \tag{1.5}$$

Based on rigid body equilibrium, the transformation from basic to local forces is defined as

$$\mathbf{a}_{bl}^T = \begin{bmatrix} -1 & 0 & 0 & 0 & 0 & 0 \\ 0 & \frac{1}{L} & \frac{1}{L} & 0 & 0 & 0 \\ 0 & 0 & 0 & -\frac{1}{L} & -\frac{1}{L} & 0 \\ 0 & 0 & 0 & 0 & 0 & -1 \\ 0 & 0 & 0 & 1 & 0 & 0 \\ 0 & 1 & 0 & 0 & 0 & 0 \\ 1 & 0 & 0 & 0 & 0 & 0 \\ 0 & -\frac{1}{L} & -\frac{1}{L} & 0 & 0 & 0 \\ 0 & 0 & 0 & \frac{1}{L} & \frac{1}{L} & 0 \\ 0 & 0 & 0 & 0 & 0 & 1 \\ 0 & 0 & 0 & 0 & 1 & 0 \\ 0 & 0 & 1 & 0 & 0 & 0 \end{bmatrix} \tag{1.6}$$

where the equilibrium relationship is

$$\mathbf{p}_l = \mathbf{a}_{bl}^T\mathbf{p}_b + \mathbf{p}_{lw} \tag{1.7}$$

where the vector $\mathbf{p}_{lw}$ accounts for the effects of member loads as "reactions" on the basic system. For the case of uniform distributed loads w_x, w_y, and w_z acting on the pipe element along the local x, y, and z axes, respectively, the local forces due to member loads are

$$\mathbf{p}_{lw} = \begin{bmatrix} -w_xL & -w_yL/2 & -w_zL/2 & 0 & 0 & 0 & 0 & -w_yL/2 & -w_zL/2 & 0 & 0 & 0 \end{bmatrix}^T \tag{1.8}$$

Assuming small displacement, first order geometry between displacements in the local and basic systems is described by the transpose of the equilibrium relationship

$$\mathbf{u}_b = \mathbf{a}_{bl}\mathbf{u}_l \tag{1.9}$$

1.2 Section level

At every location along a pipe element, the internal state consists of axial, flexural, shear, and torsion forces, collected in a section force vector

$$\mathbf{s} = \begin{bmatrix} N & M_z & M_y & T & V_y & V_z \end{bmatrix}^T \tag{1.10}$$

Based on equilibrium within the basic system, the section forces can be expressed as the sum of homogeneous and particular solutions to the differential equations of beam equilibrium

$$\mathbf{s} = \mathbf{b}\mathbf{p}_b + \mathbf{s}_p \tag{1.11}$$

where the equilibrium matrix represents the homogeneous solution due to basic forces

$$\mathbf{b} = \begin{bmatrix} 1 & 0 & 0 & 0 & 0 & 0 \\ 0 & \frac{x}{L} - 1 & \frac{x}{L} & 0 & 0 & 0 \\ 0 & 0 & 0 & \frac{x}{L} - 1 & \frac{x}{L} & 0 \\ 0 & 0 & 0 & 0 & 0 & 1 \\ 0 & \frac{1}{L} & \frac{1}{L} & 0 & 0 & 0 \\ 0 & 0 & 0 & \frac{1}{L} & \frac{1}{L} & 0 \end{bmatrix} \tag{1.12}$$

and the vector $\mathbf{s}_p$ represents the particular solution due to member loads. For the case of uniform distributed loads w_x, w_y, and w_z acting along the local x, y, and z axes, respectively, the particular solution is

$$\mathbf{s}_p = \begin{bmatrix} w_x(L-x) \\ \frac{w_y}{2} x(x-L) \\ \frac{w_z}{2} x(L-x) \\ 0 \\ w_y(x - L/2) \\ w_z(L/2 - x) \end{bmatrix} \tag{1.13}$$

Conjugate to the forces at every section along the pipe are the axial deformation, curvature, shear deformation, and twist, collected in the vector, $\mathbf{e}$

$$\mathbf{e} = \begin{bmatrix} \varepsilon_a & \kappa_z & \kappa_y & \phi & \gamma_y & \gamma_z \end{bmatrix}^T \tag{1.14}$$

Assuming linear-elastic material response described by modulus, E, and Poisson ratio, ν, the section force-deformation constitutive relationship is

$$\mathbf{s} = \mathbf{K}_s \mathbf{e} \tag{1.15}$$

where $\mathbf{K}_s$ is the section stiffness matrix. For the common case where the origin of the section y-z coincides with the with the geometric center of the pipe section, section stiffness matrix is diagonal

$$\mathbf{K}_s = \begin{bmatrix} EA & & & & & \\ & EI_z & & & & \\ & & EI_y & & & \\ & & & GJ & & \\ & & & & GA_{vy} & \\ & & & & & GA_{vz} \end{bmatrix} \tag{1.16}$$

where A is the pipe cross-section area and A_{vy} and A_{vz} are the shear areas along the y and z directions, respectively. The second moment of pipe area about the z and y axes are denoted by I_z and I_y, respectively, and J is the polar moment of the pipe section area. Note that $I_y = I_z$ and $A_{vy} = A_{vz}$ for a circular pipe. The shear modulus, G, is computed from the elastic modulus and Poisson ratio as $G = 0.5E/(1+\nu)$.

Due to the diagonal form of the section stiffness matrix, it is straightforward to find the section flexibility matrix, $\mathbf{f}_s$, in closed form by inverting each diagonal term

$$\mathbf{f}_s = \mathbf{K}_s^{-1} \begin{bmatrix} 1/(EA) & & & & & & \\ & 1/(EI_z) & & & & & \\ & & 1/(EI_y) & & & & \\ & & & 1/(GJ) & & & \\ & & & & 1/(GA_{vy}) & & \\ & & & & & 1/(GA_{vz}) & \end{bmatrix} \tag{1.17}$$

With the section flexibility matrix, the section deformations can be expressed in terms of section forces

$$\mathbf{e} = \mathbf{f}_s \mathbf{s} \tag{1.18}$$

1.3 Element formulation

Based on the principle of virtual forces, the compatibility relationship between section deformations along the pipe and the basic deformations at the ends of the pipe is expressed in integral form

$$\mathbf{u}_b = \int_0^L \mathbf{b}^T \mathbf{e}\, dx \tag{1.19}$$

Combining the compatibility relationship with the section force-deformation relationship (Eq. (1.18)) and the element equilibrium relationship (Eq. (1.11)) gives the element force-deformation relationship in the basic system

$$\mathbf{u}_b = \mathbf{f}_b \mathbf{p}_b + \mathbf{u}_{b0} \tag{1.20}$$

where $\mathbf{f}_b$ is the basic flexibility matrix and $\mathbf{u}_b$ is the vector of deformations due to member loads and other load effects such as temperature and pressure.

The element flexibility matrix is

$$\mathbf{f}_b = \int_0^L \mathbf{b}^T \mathbf{f}_s \mathbf{b}\, dx \tag{1.21}$$

For the section flexibility matrix defined in Eq. (1.17) and the equilibrium matrix of Eq. (1.12), the integral of the matrix triple product can be evaluated in closed form

$$\mathbf{f}_b = \begin{bmatrix} \frac{L}{EA} & & & & & & \\ & \frac{a_1 L}{3EI_z} & -\frac{b_1 L}{6EI_z} & & & & \\ & -\frac{b_1 L}{6EI_z} & \frac{a_1 L}{3EI_z} & & & & \\ & & & \frac{a_2 L}{3EI_y} & -\frac{b_2 L}{6EI_y} & & \\ & & & -\frac{b_2 L}{6EI_y} & \frac{a_2 L}{3EI_y} & & \\ & & & & & \frac{L}{GJ} & \end{bmatrix} \tag{1.22}$$

where the a and b coefficient account for the flexural stiffness of the section relative to the section shear stiffness

$$\begin{aligned} a_1 &= 1 + \frac{3EI_z}{GA_{vy}L^2} \\ b_1 &= 1 - \frac{6EI_z}{GA_{vy}L^2} \\ a_2 &= 1 + \frac{3EI_y}{GA_{vz}L^2} \\ b_2 &= 1 - \frac{6EI_z}{GA_{vz}L^2} \end{aligned} \tag{1.23}$$

For a circular pipe, $a_1 = a_2$ and $b_1 = b_2$.

The vector of element deformations due to member loads in Eq. (1.20) is defined in terms of the section flexibility matrix and particular solution to beam equilibrium

$$\mathbf{u}_{b0} = \int_0^L \mathbf{b}^T \mathbf{f}_s \mathbf{s}_p \, dx \tag{1.24}$$

Like the element flexibility, the vector of deformations due to member loads can be evaluated in closed form

$$\mathbf{u}_{b0} = \begin{bmatrix} \frac{w_x L^2}{2EA} \\ \frac{w_y L^3}{24EI_z} \\ -\frac{w_y L^3}{24EI_z} \\ -\frac{w_z L^3}{24EI_y} \\ \frac{w_z L^3}{24EI_y} \\ 0 \end{bmatrix} \tag{1.25}$$

where it is noted that the effect of shear deformation is not present for the case of uniform distributed transverse loads.

To incorporate the pipe element in standard displacement-based finite element analyses where element contributions to stiffness and residual forces are assembled, the element force-deformation relationship of Eq. (1.20) is expressed as basic forces in terms of basic deformations via basic stiffness

$$\mathbf{p}_b = \mathbf{k}_b \mathbf{u}_b + \mathbf{p}_{b0} \tag{1.26}$$

where the basic stiffness matrix is the inverse of the element flexibility defined in Eq. (1.22)

$$\mathbf{k}_b = \begin{bmatrix} \frac{EA}{L} & & & & & & \\ & B_1 \frac{4EI_z}{L} & C_1 \frac{2EI_z}{L} & & & & \\ & C_1 \frac{2EI_z}{L} & B_1 \frac{4EI_z}{L} & & & & \\ & & & B_2 \frac{4EI_y}{L} & C_2 \frac{2EI_y}{L} & & \\ & & & C_2 \frac{2EI_y}{L} & B_2 \frac{4EI_y}{L} & & \\ & & & & & \frac{GJ}{L} \end{bmatrix} \tag{1.27}$$

where the coefficients account for flexural stiffness relative to shear stiffness

$$\begin{aligned} B_1 &= \frac{3a_1}{4a_1^2 - b_1^2} \\ C_1 &= \frac{3b_1}{4a_1^2 - b_1^2} \\ B_2 &= \frac{3a_2}{4a_2^2 - b_2^2} \\ C_2 &= \frac{3b_2}{4a_2^2 - b_2^2} \end{aligned} \tag{1.28}$$

Note that when shear deformations are neglected, $B = C = 1$.

The second term in Eq. (1.26) is the fixed-end basic force vector

$$\mathbf{p}_{b0} = -\mathbf{k}_b \mathbf{u}_{b0} \tag{1.29}$$

Considering only uniform distributed loads, the fixed-end basic forces are

$$\mathbf{p}_{b0} = \begin{bmatrix} -\frac{w_x L}{2} \\ -\frac{w_y L^2}{12} \\ \frac{w_y L^2}{12} \\ \frac{w_z L^2}{12} \\ -\frac{w_z L^2}{12} \\ 0 \end{bmatrix} \tag{1.30}$$

Finally, for assembly into the global equilibrium equations of a finite element analysis, the element force-deformation response is transformed from the basic system to the global DOFs via matrix-matrix and matrix-vector multiplication. In the global DOFs, the element stiffness matrix is obtained from the local-basic and global-local transformation matrices

$$\mathbf{k} = \mathbf{a}_{lg}^T \mathbf{a}_{bl}^T \mathbf{k}_b \mathbf{a}_{bl} \mathbf{a}_{lg} \tag{1.31}$$

while the effect of member loads on the element forces in the global DOFs is obtained from the effects of member loads in the basic and local systems

$$\mathbf{p}_0 = \mathbf{a}_{lg}^T \left(\mathbf{a}_{bl}^T \mathbf{p}_{b0} + \mathbf{p}_{lw} \right) \tag{1.32}$$

1.4 Thermal Expansion and Internal Pressure

Uniform thermal expansion and internal pressure are additional non-mechanical load effects that must be accounted for in pipe elements. Both of these effects affect only the axial deformation at each section along a pipe element.

The additional axial deformation of a pipe section due to uniform thermal expansion is

$$\varepsilon_{thermal} = \alpha \Delta T \tag{1.33}$$

where α is the coefficient of thermal expansion for the pipe material and ΔT is the change in temperature (relative to ambient conditions).

Likewise, the additional axial deformation of a pipe section due to uniform internal pressure is

$$\varepsilon_{pressure} = p_o \frac{(D_o - t)(1 - 2\nu)}{4Et} \tag{1.34}$$

where p_o is the internal pressure and D_o and t are the pipe diameter and wall thickness, respectively. Then, the total element deformations due uniform distributed loads, uniform thermal expansion, and internal pressure is

$$\mathbf{u}'_{b0} = \mathbf{u}_{b0} + \begin{bmatrix} \alpha \Delta T L + \frac{p_0 (D_0 - t)(1-2\nu) L}{4Et} \\ 0 \\ 0 \\ 0 \\ 0 \\ 0 \end{bmatrix} \tag{1.35}$$

where $\mathbf{u}_{b0}$ is the vector of deformations due to mechanical loads. Then, the total fixed-end basic forces considering all load effects is

$$\mathbf{p}_{b0} = \begin{bmatrix} -\frac{w_x L}{2} - \alpha \Delta T E A - \frac{p_0 (D_0 - t)(1-2\nu) A}{4t} \\ -\frac{w_y L^2}{12} \\ \frac{w_y L^2}{12} \\ \frac{w_z L^2}{12} \\ -\frac{w_z L^2}{12} \\ 0 \end{bmatrix} \tag{1.36}$$

Thermal expansion and internal pressure do not affect the vector of local forces, $\mathbf{p}_{lw}$.

Chapter 2

Formulation for 3D curved pipe element

Like the straight pipe element, the curved pipe element is formulated using basic, local, and global coordinate systems [4]. Additional details of the curve pipe element for internal pressure and thermal effects are based on [1] and accompanying SAP source code obtained from NISEE [8]. All symbolic calculations for the curved pipe formulation can be found in the `Report.ipynb` file included with this report.

2.1 Global, local, and basic systems

Like a straight pipe element, a curved pipe element is defined by two end nodes, I and J, with 12 global DOFs, as shown in Figure 2.1. Degrees of freedom 1-6 are defined at end I while DOFs 7-12 are defined at end J, with DOFs 1-3 and 7-9 as translations (forces) and DOFs 4-6 and 10-12 as rotations (moments).

The local system for a curved pipe element is defined by the x-axis, which points from end I to end J and the vector y, which lies in the plane of the element, while he local z-axis is perpendicular to the plane that contains the element. As shown in Figure 2.2, the 12 local DOFs coincide with the local axes.

With the definition of the global and local systems for a curved pipe element, the transformation of displacement and forces between the global and local systems is the same as that for the straight element in Eq. (1.1). The same local DOFs are selection for the basic system of a curved element as for straight pipe elements defined in Eq. (1.5).

The curved pipe element is shown in the local x-y and x-z planes in Fig.2.3. In the x-y plane, which contains the element curve, C is the center point for the curve, R is the radius of curvature, and θ_0 is the half angle of the curve. The variable, L, is defined as the chord distance between ends I and J, and can be expressed in terms of the pipe radius or curvature and the half angle

$$L = 2R \sin \theta_0 \tag{2.1}$$

The distance from the center of pipe curvature, C, to the element chord is expressed as

$$H_0 = R \cos \theta_0 \tag{2.2}$$

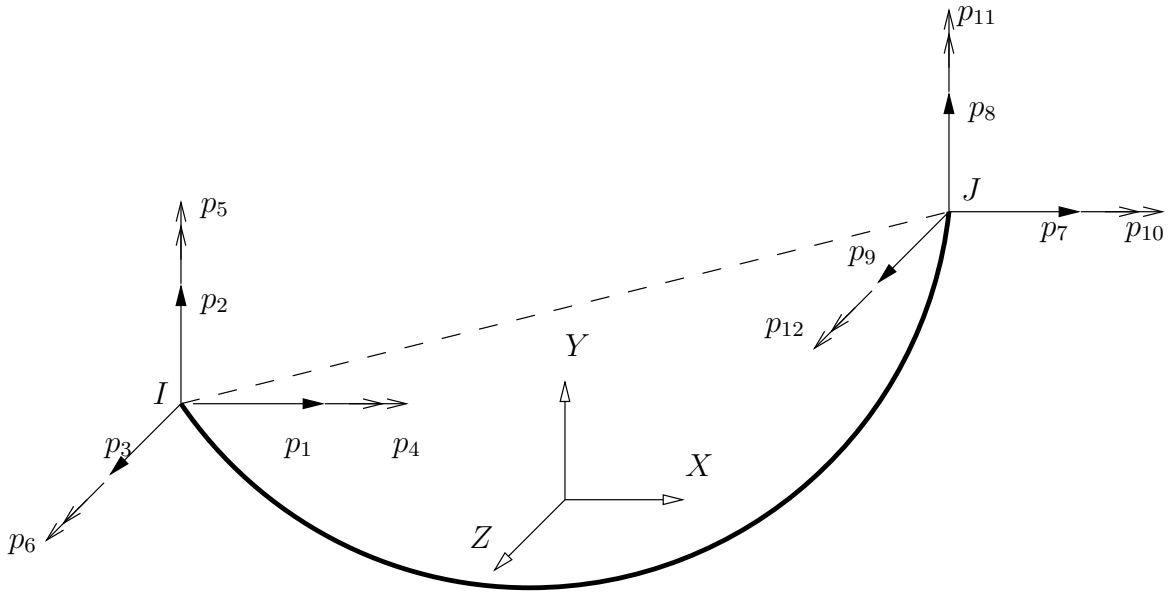

Figure 2.1: Global system for a curved pipe element in 3D.

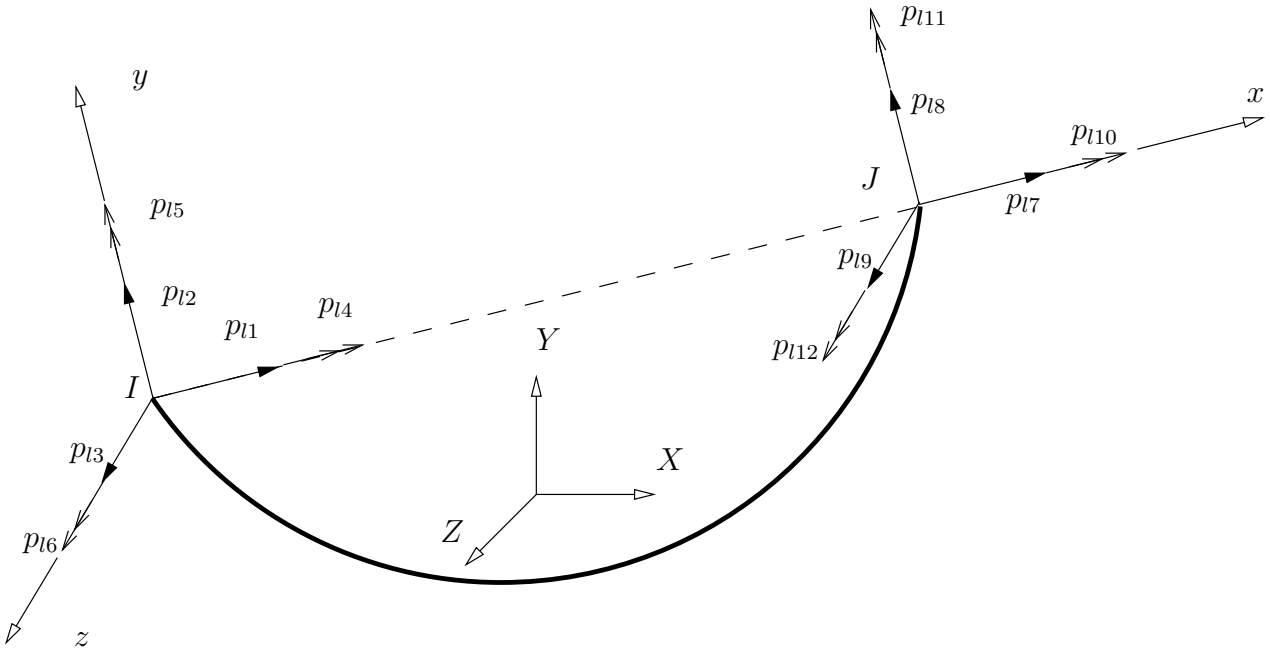

Figure 2.2: Local system for a curved pipe element in 3D.

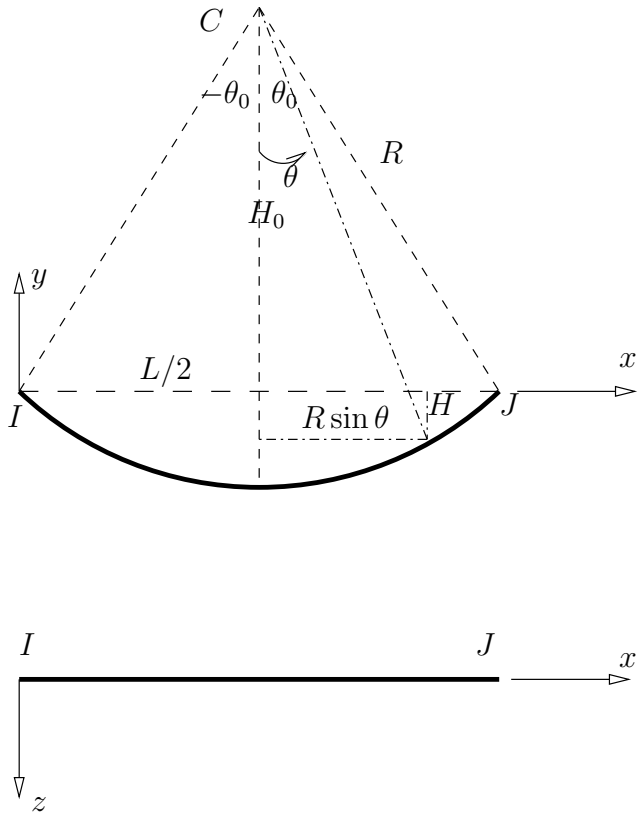

Figure 2.3: The model in local x-y and x-z planes.

while the distance from the element chord to the pipe is

$$H = R(\cos\theta - \cos\theta_0) \tag{2.3}$$

The curved pipe formulation includes uniform distributed loads, w_x, w_y, and w_z acting along the pipe arc in the directions of the local x, y, and z axes, respectively, as shown in Figure 2.4. Based on equilibrium in the local system, the sum of forces along the x-axis includes the forces in

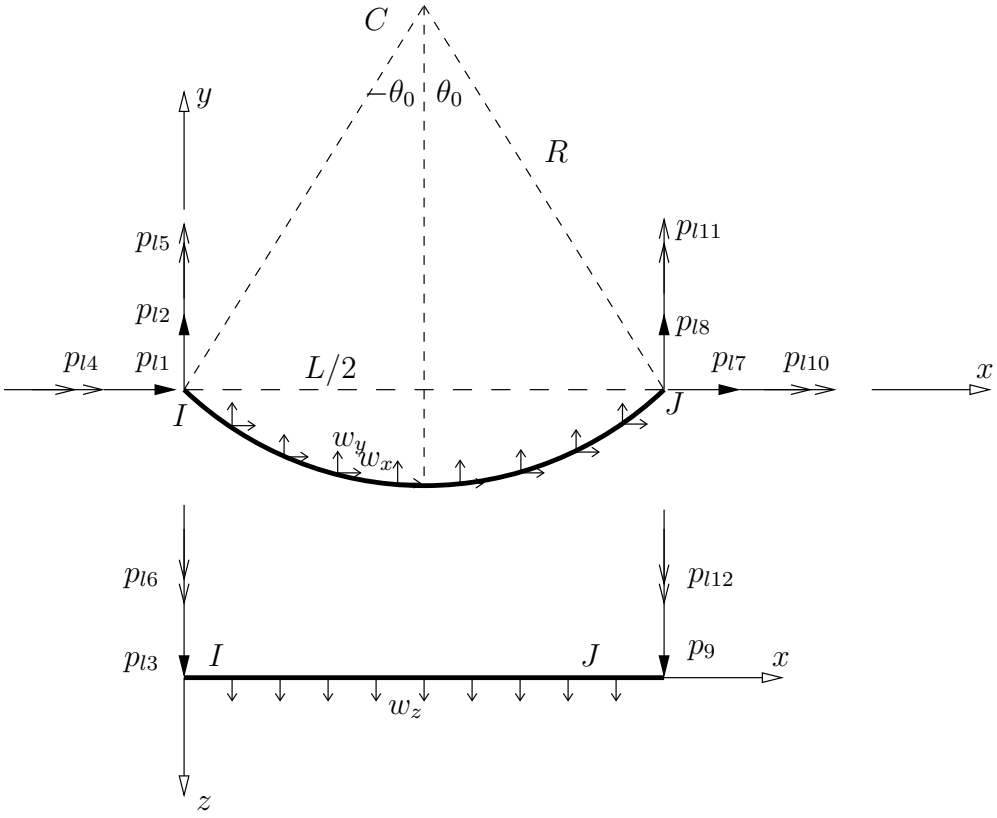

Figure 2.4: The basic local transformation in local x-y and x-z planes.

local DOFs 1 and 7 as well as the uniform distributed load integrated along the pipe arc length:

$$\sum F_x = p_{l1} + p_{l7} + \int_{-\theta_0}^{\theta_0} w_x R d\theta = p_{l1} + p_{l7} + 2w_x R\theta_0 = 0 \tag{2.4}$$

Likewise, equilibrium in the local y-direction is

$$\sum F_y = p_{l2} + p_{l8} + \int_{-\theta_0}^{\theta_0} w_y R d\theta = p_{l2} + p_{l8} + 2w_y R\theta_0 = 0 \tag{2.5}$$

while equilibrium in the local z-direction is

$$\sum F_z = p_{l3} + p_{l9} + \int_{-\theta_0}^{\theta_0} w_z R d\theta = p_{l3} + p_{l9} + 2w_z R\theta_0 = 0 \tag{2.6}$$

Moment equilibrium about the local x-axis (torque) consists of the end moments and the distributed load along the local z-axis

$$\begin{aligned}\sum M_x &= p_{l4} + p_{l10} - \int_{-\theta_0}^{\theta_0} w_z H R d\theta \\ &= p_{l4} + p_{l10} - \int_{-\theta_0}^{\theta_0} w_z R^2(\cos\theta - \cos\theta_0) d\theta \\ &= p_{l4} + p_{l10} - w_z R(L - 2\theta_0 H_0) = 0\end{aligned} \tag{2.7}$$

About the local y-axis, moment equilibrium about end I includes the end moments, the effect of shear force at end J, and the distributed load along the local z-axis

$$\begin{aligned}\sum M_{yI} &= p_{l5} + p_{l11} - p_{l9} L - \int_{-\theta_0}^{\theta_0} w_z(L/2 + R\sin\theta) R d\theta = 0 \\ &= p_{l5} + p_{l11} - p_{l9} L - w_z R L \theta_0 = 0\end{aligned} \tag{2.8}$$

Likewise, moment equilibrium about the local z-axis about end I includes end moments and shear force at J, and the distributed loads acting along the pipe arc in the x-y plane

$$\begin{aligned}\sum M_{zI} &= p_{l6} + p_{l12} + p_{l8} L + \int_{-\theta_0}^{\theta_0} w_x H R d\theta + \int_{-\theta_0}^{\theta_0} w_y(L/2 + R\sin\theta) R d\theta = 0 \\ &= p_{l6} + p_{l12} + p_{l8} L + w_x R(L - 2\theta_0 H_0) + w_y L R \theta_0 = 0\end{aligned} \tag{2.9}$$

Solving the above equilibrium equations for all local forces $\mathbf{p}_l$ in terms of basic forces $\mathbf{p}_b$ and member loads gives a matrix-vector expression identical to that for straight pipe elements

$$\mathbf{p}_l = \mathbf{a}_{bl}^T \mathbf{p}_b + \mathbf{p}_{lw} \tag{2.10}$$

where the local-basic transformation matrix, $\mathbf{a}_{bl}$, is as shown in Eq. (1.6). However, the effect of member loads contained in the vector $\mathbf{p}_{lw}$ is

$$\mathbf{p}_{lw} = \begin{bmatrix} -2w_x R\theta_0 \\ w_x R(1 - \frac{2\theta_0 H_0}{L}) - w_y R\theta_0 \\ -w_z R\theta_0 \\ w_z R(L - 2\theta_0 H_0) \\ 0 \\ 0 \\ 0 \\ -w_x R(1 - \frac{2\theta_0 H_0}{L}) - w_y R\theta_0 \\ -w_z R\theta_0 \\ 0 \\ 0 \\ 0 \end{bmatrix} \tag{2.11}$$

2.2 Section level

To express the internal section forces in terms of basic forces, a section is cut through the pipe at arbitrary angle, θ, as shown in Figure 2.5. The internal forces exposed by the cut are the axial

force, N, acting along the tangent to the pipe arc and torsion, T, acting about the tangent to the pipe arc. In addition, the shear, V_y, acts in the x-y plane and is directed away from the center of pipe curvature, C. The shear force, V_z, acts in the x-z plane. Internal bending moments M_y and M_z act about the lines of action for the corresponding shear, V_y and V_z, respectively.

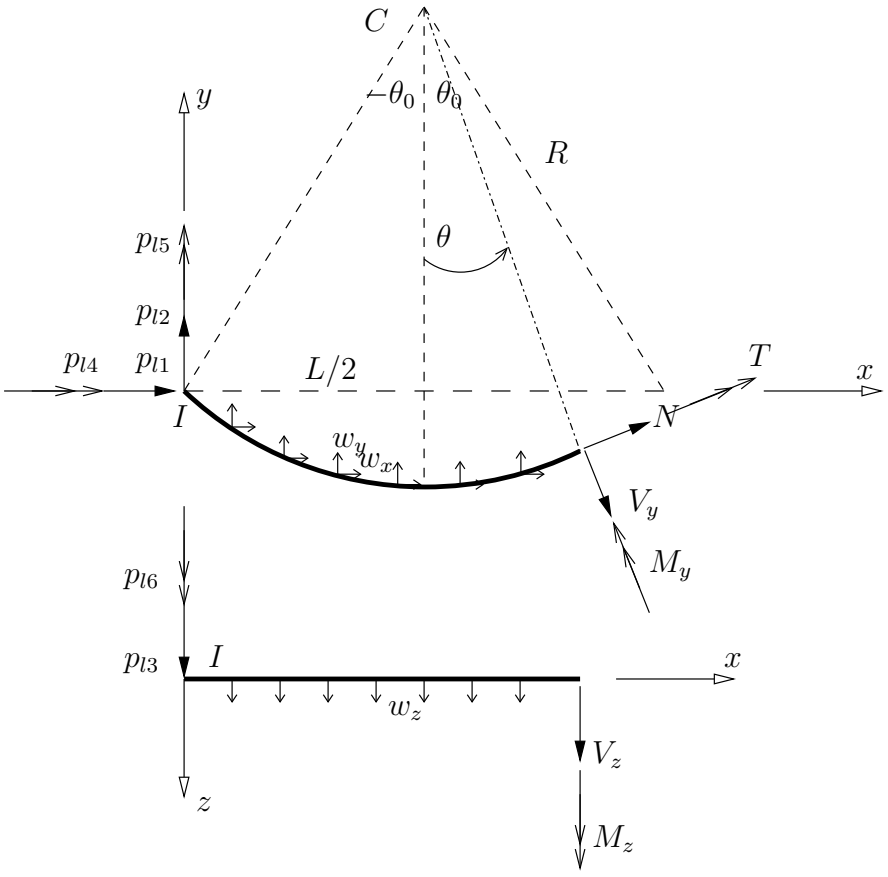

Figure 2.5: The equilibrium for sections in local x-y and x-z planes.

Equations for the internal pipe forces are based on section equilibrium with the cosine and sine, $c \equiv \cos\theta$ and $s \equiv \sin\theta$, respectively, of the half angle, θ, shown in Figure 2.5. Note that sections to the left of the half angle have $\theta < 0$ while sections to the right have $\theta > 0$.

Summing forces along the local x-direction gives the following equation relating internal axial force, N, and shear force, V_y, to the end forces and distributed loads acting in the x-y plane:

$$\sum F_x = p_{l1} + cN + sV_y + \int_{-\theta_0}^{\theta} w_x R\, dt = p_{l1} + cN + sV_y + w_x R(\theta + \theta_0) = 0 \tag{2.12}$$

where dt is a differential length along the pipe arc. Similarly, force equilibrium along the local y-axis gives

$$\sum F_y = p_{l2} + sN - cV_y + \int_{-\theta_0}^{\theta} w_y R\, dt = p_{l2} + sN - cV_y + w_y R(\theta + \theta_0) = 0 \tag{2.13}$$

Turning to the x-z plane, equilibrium of forces in the z-direction gives

$$\sum F_z = p_{l3} + V_z + \int_{-\theta_0}^{\theta} w_z R \, dt = p_{l3} + V_z + w_z R(\theta + \theta_0) = 0 \tag{2.14}$$

Moment equilibrium of the cut pipe section about the local x-axis at end I gives the following expression

$$\begin{aligned} \sum M_{xI} &= p_{l4} + cT - sM_y - V_z H - \int_{-\theta_0}^{\theta} w_z H_t R \, dt \\ &= p_{l4} + cT - sM_y - V_z H - \int_{-\theta_0}^{\theta} w_z R^2(\cos(t) - \cos\theta_0) \, dt \\ &= p_{l4} + cT - sM_y - V_z H - w_z R(Rs + L/2 - \theta H_0 - \theta_0 H_0) = 0 \end{aligned} \tag{2.15}$$

Taking moments about end I about the local y-axis gives the following expression

$$\begin{aligned} \sum M_{yI} &= p_{l5} + Ts + M_y c + p_{l3}(L/2 + Rs) + \int_{-\theta_0}^{\theta} w_z(R\sin\theta - R\sin(t))R \, dt \\ &= p_{l5} + Ts + M_y c + p_{l3}(L/2 + Rs) + w_z R^2 s(\theta + \theta_0) + w_y R(Rc - H_0) = 0 \end{aligned} \tag{2.16}$$

while, similarly, moments about the local z-axis gives

$$\begin{aligned} \sum M_{zI} =& p_{l6} + M_z - p_{l1} H - p_{l2}(L/2 + Rs) \\ & - \int_{-\theta_0}^{\theta} w_x(H - H_t)R \, dt - \int_{-\theta_0}^{\theta} w_y(R\sin\theta - R\sin(t))R \, dt \\ =& p_{l6} + M_z - p_{l1}(Rc - H_0) - p_{l2}(L/2 + Rs) \\ & - w_x R^2 c(\theta + \theta_0) + w_x R(Rs + L/2) \\ & - w_y R^2 s(\theta + \theta_0) - w_y R(Rc - H_0) = 0 \end{aligned} \tag{2.17}$$

Then, solving the six equilibrium equations for the section forces, $\mathbf{s}$, in terms of basic forces $\mathbf{p}_b$, and the effects of member loads gives the following expressions. First, axial force

$$N = cp_{b1} - \frac{s}{L}p_{b2} - \frac{s}{L}p_{b3} + w_x R(c\theta_0 - c\theta - s + \frac{2s\theta_0 H_0}{L}) - w_y Rs\theta \tag{2.18}$$

Then, shear force along the local y-axis

$$V_y = sp_{b1} + \frac{c}{L}p_{b2} + \frac{c}{L}p_{b3} + w_x R(c - s\theta + s\theta_0 - \frac{2c\theta_0 H_0}{L}) + w_y Rc\theta \tag{2.19}$$

and shear force along the local z-axis

$$\begin{aligned} V_z &= -p_{l3} - w_z R(\theta + \theta_0) \\ &= -(-\frac{1}{L}p_{b4} - \frac{1}{L}p_{b5} - w_z R\theta_0) - w_z R(\theta + \theta_0) \\ &= \frac{1}{L}p_{b4} + \frac{1}{L}p_{b5} - w_z R\theta \end{aligned} \tag{2.20}$$

The bending moment about the local z-axis is

$$\begin{aligned} M_z &= -p_{l6} + p_{l1}(Rc - H_0) + p_{l2}(L/2 + Rs) \\ &\quad + w_x R^2 c(\theta + \theta_0) - w_x R(Rs + L/2) \\ &\quad + w_y R^2 s(\theta + \theta_0) + w_y R(Rc - H_0) \\ &= -p_{b2} + (-p_{b1} - 2w_x R\theta_0)(Rc - H_0) \\ &\quad + (\frac{1}{L}p_{b2} + \frac{1}{L}p_{b3} + w_x R(1 - \frac{2\theta_0 H_0}{L}) - w_y R\theta_0)(L/2 + Rs) \\ &\quad + w_x R^2 c(\theta + \theta_0) - w_x R(Rs + L/2) \\ &\quad + w_y R^2 s(\theta + \theta_0) + w_y R(Rc - H_0) \end{aligned} \tag{2.21}$$

while the bending moment about the local y-axis is

$$\begin{aligned} M_y = (\frac{sH_0}{L} - \frac{c}{2})p_{b4} + (\frac{sH_0}{L} + \frac{c}{2})p_{b5} - sp_{b6} \\ + w_z R^2(\cos(\theta - \theta_0) - \theta_0 \sin(\theta - \theta_0) - 1) \end{aligned} \tag{2.22}$$

And finally, the torsional moment is

$$\begin{aligned} T = \frac{R}{L}(1 - \cos(\theta - \theta_0))p_{b4} + \frac{R}{L}(1 - \cos(\theta + \theta_0))p_{b5} + cp_{b6} \\ + w_z R^2(\theta_0 \cos(\theta - \theta_0) + \sin(\theta - \theta_0) - \theta) \end{aligned} \tag{2.23}$$

Similar to the straight pipe element (Eq. (1.11), the equations for section forces in terms of basic forces and member loads is expressed in the matrix-vector form

$$\mathbf{s} = \mathbf{b}\mathbf{p}_b + \mathbf{s}_p \tag{2.24}$$

The equilibrium matrix, $\mathbf{b}$, representing the homogeneous solution to curved pipe equilibrium is

$$\mathbf{b} = \begin{bmatrix} c & -\frac{s}{L} & -\frac{s}{L} & 0 & 0 & 0 \\ -H & \frac{Rs}{L} - \frac{1}{2} & \frac{Rs}{L} + \frac{1}{2} & 0 & 0 & 0 \\ 0 & 0 & 0 & \frac{sH_0}{L} - \frac{c}{2} & \frac{sH_0}{L} + \frac{c}{2} & -s \\ 0 & 0 & 0 & \frac{R}{L}(1 - \cos(\theta - \theta_0)) & \frac{R}{L}(1 - \cos(\theta + \theta_0)) & c \\ s & \frac{c}{L} & \frac{c}{L} & 0 & 0 & 0 \\ 0 & 0 & 0 & \frac{1}{L} & \frac{1}{L} & 0 \end{bmatrix} \tag{2.25}$$

while the vector, $\mathbf{s}_p$, of section forces due to member loads is

$$\mathbf{s}_p = \begin{bmatrix} w_x R(c\theta_0 - s - c\theta + \frac{2s\theta_0 H_0}{L}) - w_y Rs\theta \\ w_x R(cR\theta - \frac{2sR\theta_0 H_0}{L} - cR\theta_0 + \theta_0 H_0) + w_y R(sR\theta - \frac{\theta_0 L}{2} + cR - H_0) \\ w_z R^2(-\theta_0 \sin(\theta - \theta_0) + \cos(\theta - \theta_0) - 1) \\ w_z R^2(-\theta + \theta_0 \cos(\theta - \theta_0) + \sin(\theta - \theta_0)) \\ w_x R(c + s\theta_0 - s\theta - \frac{2c\theta_0 H_0}{L}) + w_y Rc\theta \\ -w_z R\theta \end{bmatrix} \tag{2.26}$$

2.3 Element formulation

The formulation of the curved pipe element takes the same form as the straight pipe element in that the element flexibility is integrated from the section flexibility and element equilibrium matrix

$$\mathbf{f}_b = \int_{-\theta_0}^{\theta_0} \mathbf{b}^T \mathbf{f}_s \mathbf{b} \, R d\theta \tag{2.27}$$

Instead of closed-form integration, which is straightforward for the straight pipe element, numerical integration is used to evaluate the flexibility of the curved pipe element

$$\mathbf{f}_b = \sum \mathbf{b}^T(t_i) \mathbf{f}_s(t_i) \mathbf{b}(t_i) \, R w_i \tag{2.28}$$

where t_i and w_i are the location and weight, respectively, of the i^{th} integration point.

Similar, the element deformations due to member loads

$$\mathbf{u}_{b0} = \int_0^L \mathbf{b}^T \mathbf{f}_s \mathbf{s}_p \, dt \tag{2.29}$$

is also evaluated by numerical, rather than closed-form, integration for the curved pipe element.

$$\mathbf{u}_{b0} = \sum \mathbf{b}^T(t_i) \mathbf{f}_s(t_i) \mathbf{s}_p(t_i) \, w_i \tag{2.30}$$

For both the element flexibility, $\mathbf{f}_b$, and the initial deformations, $\mathbf{u}_{b0}$, 20 Gauss-points are mapped onto the element arc in order to perform numerical integration.

After numerically integrating the element flexibility and initial deformations, the element basic force-deformation relationship is evaluated

$$\mathbf{p}_b = \mathbf{k}_b \mathbf{u}_b + \mathbf{p}_{b0} \tag{2.31}$$

where $\mathbf{k}_b$ is the inverse of the element flexibility, i.e., $\mathbf{k}_b = \mathbf{f}_b^{-1}$. The vector of fixed-end basic forces is then evaluated as the matrix-vector product

$$\mathbf{p}_{b0} = -\mathbf{k}_b \mathbf{u}_{b0} \tag{2.32}$$

With the basic force-deformation relationship, the transformation of forces and stiffness from the basic system up to the local system follows the local-basic transformation matrix, $\mathbf{a}_{bl}$, and the rigid body effects of member loads, $\mathbf{p}_{lw}$. Then, transformation to the global system follows the same procedure as the straight pipe element via the local x, y, and z axes in the $\mathbf{a}_{lg}$ matrix.

2.4 Thermal expansion and internal pressure

Compared to the straight pipe, the effects of thermal expansion and internal pressure for curved pipes are more complicated with additional terms in the $\mathbf{u}_{b0}$ vector. Thermal expansion causes axial elongation while internal pressure leads to axial elongation as well as curvature about the local z-axis.

$$\mathbf{e}_0 = \begin{bmatrix} \alpha \Delta T + \frac{p_0 (D_0 - t)(1 - 2\nu)}{4Et} \\ \kappa_{z0} \\ 0 \\ 0 \\ 0 \\ 0 \end{bmatrix} \tag{2.33}$$

The axial strain is due to thermal expansion and internal pressure is the same as that for the straight pipe element. However, the additional curvature due to internal pressure is

$$\kappa_{z0} = -\frac{\pi p_0}{2REI_z}\left(\frac{D_0 - t}{2}\right)^4 \left[2 - 2\nu + (3 + 1.5\nu)\left(\frac{D_0 - t}{2R}\right)^2\right] \tag{2.34}$$

Because the internal pressure is constant, the associated basic deformation can be evaluated by closed-form integration with polar coordinates

$$\mathbf{u}_{b0}^{tp} = \int_{-\theta_0}^{\theta_0} \mathbf{b}^T \mathbf{e}_0 R \, d\theta \tag{2.35}$$

After integration, the combined effects of thermal expansion and internal pressure are

$$\mathbf{u}_{b0}^{tp} = \begin{bmatrix} 2R\alpha\Delta T \sin(\theta_0) + \frac{p_0 R(D_0 - t)(1-2\nu)\sin(\theta_0)}{2Et} + 2R^2\kappa_{z0}(\theta_0 \cos(\theta_0) - \sin(\theta_0)) \\ -R\kappa_{z0}\theta_0 \\ R\kappa_{z0}\theta_0 \\ 0 \\ 0 \\ 0 \end{bmatrix} \tag{2.36}$$

and the total basic deformation becomes

$$\mathbf{u}'_{b0} = \mathbf{u}_{bo} + \mathbf{u}_{b0}^{tp} \tag{2.37}$$

which can then be used to evaluate the fixed-end basic forces via $\mathbf{p}_{b0} = -\mathbf{k}_b \mathbf{u}_{b0}$.

The ovalization effect of the curved pipe with no internal pressure is taken into account by a factor, k, as

$$k = \frac{1.65}{h} \geq 1 \tag{2.38}$$

which increases only the flexural flexibility terms, $1/EI_z$ and $1/EI_y$, of the pipe section, i.e., k/EI_z and k/EI_y, giving flexural stiffness terms EI_z/k and EI_y/k.

With internal pressure, p_0, in a curved pipe, the ovalization effect is described by a factor, k_p, which is similar to k

$$k_p = \frac{1.65/h}{1 + (6p_0/(Eh))(R/t)^{4/3}} \geq 1 \tag{2.39}$$

where

$$h = tR/r^2$$
$$r = (d_o - t)/2$$

Just like k, the factor, k_p, affects only the flexural stiffness of the pipe via EI_z/k_p and EI_y/k_p.

2.5 Tangent intersection point

In Figure 2.3, if the intersection point T of the tangents at node I and node J is given instead of center C, the following procedure calculates the center point C in terms of points I, J, and T.

Assume that the global coordinates for I, J, and T, (X_I, Y_I, Z_I), (X_J, Y_J, Z_J), and (X_T, Y_T, Z_T) respectively, are known from user input. Then the coordinates of the center point, (X_C, Y_C, Z_C), can be solved using the linear system of equations

$$\begin{bmatrix} X_T - X_I & Y_T - Y_I & Z_T - Z_I \\ X_T - X_J & Y_T - Y_J & Z_T - Z_J \\ n_x & n_y & n_z \end{bmatrix} \begin{bmatrix} X_C \\ Y_C \\ Z_C \end{bmatrix} = \begin{bmatrix} X_I(X_T - X_I) + Y_I(Y_T - Y_I) + Z_I(Z_T - Z_I) \\ X_J(X_T - X_J) + Y_J(Y_T - Y_J) + Z_J(Z_T - Z_J) \\ X_T n_x + Y_T n_y + Z_T n_z \end{bmatrix} \tag{2.40}$$

where (n_x, n_y, n_z) is the unit vector perpendicular to the plane formed by I, J, and T. The system will have a solution if points I, J, and T are not colinear.

Chapter 3

OpenSees Commands for pipe elements

3.1 Command for pipe material

```
ops.uniaxialMaterial('Pipe', matTag, nt, T1, E1, xnu1, alpT1,
                     <T2, E2, xnu2, alpT2, ... >)
```

matTag a unique tag for the material

nt the number of temperature points for the material. If two or more points are provided, the expected range of average temperatures in the element must be covered. The material properties will be interpolated among the points based on the average temperature.

T1 the temperature for point 1, T_1

E1 the Young's modulus for point 1, E_1

xnu1 the Poisson's ratio for point 1, ν_1

alpT1 the thermal expansion coefficient for point 1, α_1

3.2 Command for pipe section

```
ops.section('Pipe', secTag, do, t, <'-alphaV', alphaV>,
            <'-defaultAlphaV'>, <'-rho', rho>)
```

secTag a unique tag for the section

do the outside diameter of the pipe, d_o

t the thickness of the pipe wall, t

alphaV the shape factor, α_V, for shear distortion and must follow the option `'-alphaV'`. This is optional to be set by the user.

-defaultAlphaV use the option `'-defaultAlphaV'` to set the shape factor to the default value

$$\alpha_V = \frac{4}{3}\frac{r_o^3 - r_i^3}{(r_o^2 + r_i^2)(r_o - r_i)}$$

where $r_o = d_o/2$ and $r_i = r_o - t$. If neither `'-alphaV'` nor `'-defaultAlphaV'` is used, the shear distortion is ignored.

rho the mass per unit length of the section, ρ, which is used as mass coefficient in the dynamic analysis and will not be used to apply the gravity load, which should be added using the `ops.eleLoad` command. Default is `0`.

3.3 Command for straight pipe element

```
ops.element('Pipe', eleTag, ndI, ndJ, pipeMatTag, pipeSecTag,
            <'-T0', T0>, <'-p', p>, <'-noThermalLoad'>, <'-noPressureLoad'>)
```

eleTag a unique tag for the element

ndI tag for the node I

ndJ tag for the node J

pipeMatTag the tag for the pipe material for the element

pipeSecTag the tag for the pipe section for the element

T0 the stress-free temperature, T_0, which must follow the option `'-T0'` and will be added to the average temperature for the element. Default is `0`.

p the internal pressure, p, which must follow the option `'-p'`. The internal pressure will affect the axial deformation for the straight pipe element as shown in Sec. 1.4. Default is `0`.

-noThermalLoad Do not include the load due to thermal effects. Default is to include.

-noPressureLoad Do not include the load due to internal pressure effects. The stiffness due to internal pressure will still be included. Default is to include.

3.4 Command for curved pipe element

```
ops.element('CurvedPipe', eleTag, ndI, ndJ, pipeMatTag, pipeSecTag,
            xC, yC, zC, <'-TI'>,
            <'-T0', T0>, <'-p', p>, <'-tolWall', tolWall>,
            <'-noThermalLoad'>, <'-noPressureLoad'>)
```

eleTag a unique tag for the element

ndI tag for the node I

ndJ tag for the node J

pipeMatTag the tag for the pipe material for the element

pipeSecTag the tag for the pipe section for the element

xC, yC, zC the coordinates for the center of the curve or the tangent intersection point if the option `'-TI'` is given.

-TI if the option `'-TI'` is provided, the coordinates `[xC, yC, zC]` are for the tangent intersection point, which will be converted internally to the coordinates of the center point.

T0 the stress-free temperature, T_0, which must follow the option `'-T0'` and will be added to the average temperature for the element. Default is `0`.

p the internal pressure, p, which must follow the option `'-p'`. The internal pressure will affect the axial deformation, the curvature, and the flexibility for the curved pipe element as shown in Sec. 2.4. Default is `0`.

-tolWall the tolerance for checking radius and the optional interaction point as a fraction of wall thickness and must follow the option `'-tolWall'`. Default is `0.1`.

-noThermalLoad Do not include the load due to thermal effects. Default is to include.

-noPressureLoad Do not include the load due to internal pressure effects. The stiffness due to internal pressure will still be included. Default is to include.

3.5 Command for nodal temperature

```
ops.setNodeTemperature(nodeTag, value)
```

nodeTag tag for the node

value the temperature value for the node. The nodal temperature will affect the thermal expansion for both straight and curved pipe elements as shown in Secs. 1.4 and 2.4.

3.6 Command for element load

Only the uniform load is accepted by the pipe elements for applying the gravity load. Different to regular element loads, the load values are interpreted in the global coordinate system as it's convenient for the curved pipe elements.

```
ops.eleLoad('-ele', *eleTags, '-type', '-beamUniform', wy, wz, wx)
```

eleTags must follow the option `'-ele'` and is a list of element tags.

-type and -beamUniform the options `'-type'` and `'-beamUniform'` must follow the element tags.

wy the member load per length in the global y axis.

wz the member load per length in the global z axis.

wx the member load per length in the global x axis.

3.7 Command for element response

```
# N, Vy, Vz, T, My Mz
res = ops.eleResponse(ele, 'sectionI')
res = ops.eleResponse(ele, 'sectionC')
res = ops.eleResponse(ele, 'sectionJ')
res = ops.eleResponse(ele, 'sectionX', perc)
```

where the commands above return the section forces at node I, center, node J, or any section X. The sign conventions for the section forces are shown in Fig. 2.5.

`perc = -1`: section I, i.e. $\theta = -\theta_0$

`perc = 0`: center section, i.e. $\theta = 0$

`perc = 1`: section J, i.e. $\theta = \theta_0$

Other `perc`: section at $\theta = perc * \theta_0$

Chapter 4

BM3 Pipe Network Example

Direct integration, dynamic response history analysis is performed with the straight and curved pipe elements in OpenSeesPy for the BM3 pipe network model from NUREG/CR-6645 (BNL-NUREG-52576) [2]. The analyses in the NUREG report used "a BNL version of SAP V adapted for piping analysis".

4.1 Model Description

The BM3 pipe network shown in Figure 4.1 consists of 37 pipe elements. The model has 27 straight and 10 curved pipe elements with tags 2, 5, 7, 13, 16, 19, 23, 26, 29, and 35–all other tags correspond to straight pipe elements. The nominal diameter of elements 1–20 is 3 inches, while the nominal diameters of elements 21–30 and 31–37 are 4 inches and 8 inches, respectively. The pipe network has fixed supports at nodes 1, 31, and 38 and there are flexible supports at nodes 4, 7, 11, 15, 17, 23, and 36 with the following stiffnesses.

- Node 4 – Translation X and Z, stiffness k=1.0e8 lb/in
- Node 7 – Translation Y, stiffness k=1.0e8 lb/in
- Node 11 – Translation Y, stiffness k=1.0e8 lb/in; Translation Z, stiffness k=1.0e5 lb/in
- Node 15 – Translation X, stiffness k=1.0e5 lb/in
- Node 17 – Translation Y, stiffness k=1.0e8 lb/in; Translation Z, stiffness k=1.0e5 lb/in
- Node 23 – Translation X, stiffness k=1.0e5 lb/in; Translation Y, stiffness k=1.0e8 lb/in
- Node 36 – Translation Y, stiffness k=1.0e8 lb/in; Translation Z, stiffness k=1.0e5 lb/in

To match the SAP V analysis from the NUREG report, the OpenSees model used stiff springs at the fixed supports (nodes 1, 31, and 38) with stiffness 1.0e11 lb/in for the translational DOFs and 1.0e20 lb-in/rad for the rotational DOFs.

All pipe elements have elastic modulus, E=29.0e6 psi, Poisson ratio, ν=0.3, and coefficient of thermal expansion, α=6.44e-6/°C. Based on the pipe diameter and wall thickness, the element mass density (per unit length) is 2.324e-3 (lb-s^2/in)/in for elements 1–20 and 3.514e-3 and 1.0836e-2 for

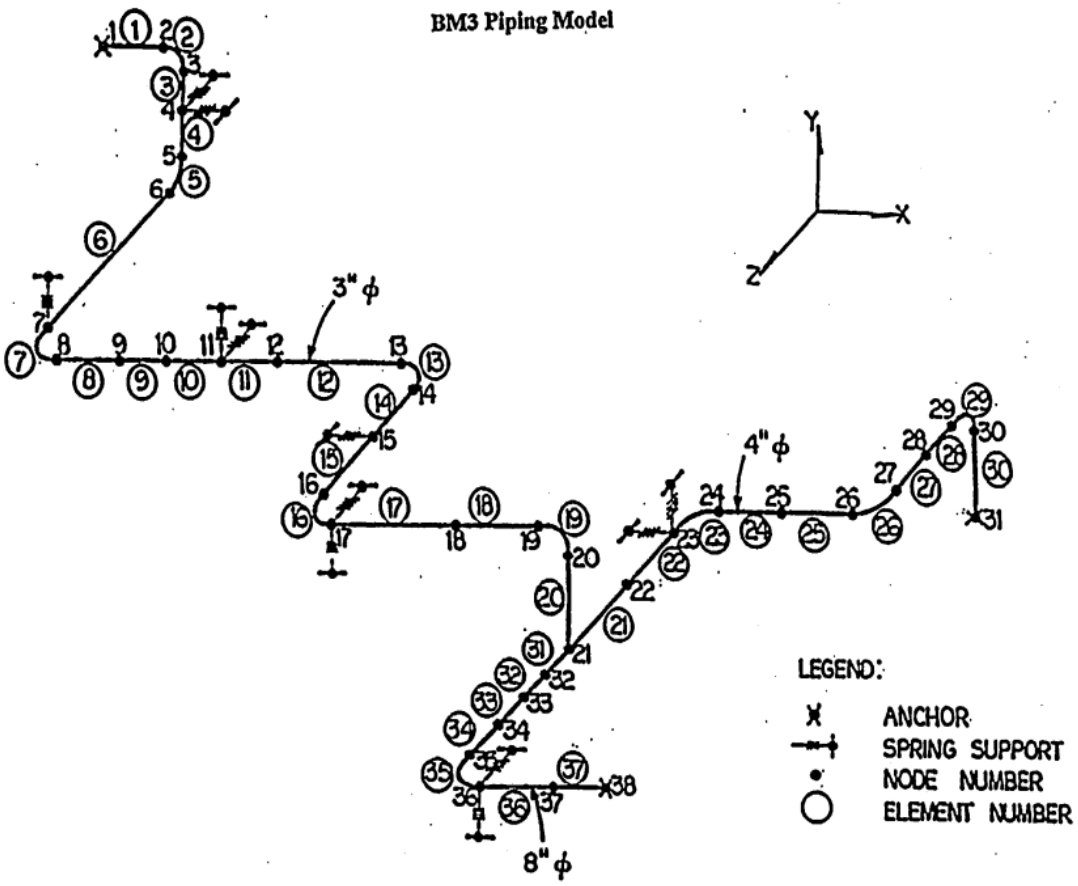

Figure 4.1: Elements, nodes, and boundary conditions for BM3 pipe network model (from NUREG/CR-6645).

elements 21–30 and 31–37, respectively. Additional details on the material properties and support conditions of the BM3 pipe model can be found in the `bm3.py` OpenSees script.

The mass of the BM3 model is developed from the pipe elements, i.e., there are no concentrated masses in the model. The nodal masses assembled from the pipe elements of the OpenSees model are compared to the nodal masses listed for the SAP V model from the NUREG report in Table 4.1. The nodal masses for the two models match to the number of significant digits shown in the NUREG report.

Having established identical mass distributions between the OpenSeesPy and SAP V models, the stiffness distribution is checked next using eigenvalue analysis. Although the BM3 model has more than 31 modes of vibration, the NUREG report listed 31 modes. Natural circular frequencies for the first 31 modes of the BM3 model are shown in Table 4.2 for SAP V (as reported in the NUREG report) and OpenSees. The natural frequencies obtained from OpenSees match the frequencies reported in the NUREG report, establishing that the mass and stiffness distributions are identical between the SAP and OpenSees models.

Table 4.1: Comparison of nodal masses from SAP V (un-numbered table on page A-9 of NUREG report) and OpenSeesPy models (units = lb-sec^2/inch)

Node	**SAP V**	**OpenSees**
1	0.017	0.017
2	0.026	0.026
3	0.212	0.212
4	0.227	0.227
5	0.031	0.031
6	0.165	0.165
7	0.165	0.165
8	0.092	0.092
9	0.267	0.267
10	0.275	0.275
11	0.182	0.182
12	0.174	0.174
13	0.092	0.092
14	0.059	0.059
15	0.101	0.101
16	0.059	0.059
17	0.105	0.105
18	0.268	0.268
19	0.180	0.180
20	0.073	0.073
21	0.207	0.207
22	0.088	0.088
23	0.043	0.043
24	0.052	0.052
25	0.197	0.197
26	0.178	0.178
27	0.048	0.048
28	0.063	0.063
29	0.048	0.048
30	0.175	0.175
31	0.158	0.158
32	0.163	0.163
33	0.276	0.276
34	0.780	0.780
35	0.687	0.687
36	0.687	0.687
37	1.170	1.170
38	0.585	0.585

Table 4.2: Comparison of natural circular frequencies, ω_n, from SAP V (un-numbered table on page A-10 of NUREG report) and OpenSeesPy (units = rad/sec)

Mode	**SAP V**	**OpenSees**	**Relative Diff**
1	18.27	18.27	0.00%
2	27.57	27.56	-0.00%
3	34.66	34.66	-0.00%
4	35.84	35.84	-0.00%
5	43.84	43.84	-0.00%
6	46.14	46.14	0.00%
7	49.51	49.51	0.00%
8	64.73	64.73	0.00%
9	69.47	69.47	0.00%
10	70.58	70.58	0.00%
11	72.24	72.24	0.00%
12	78.1	78.1	0.00%
13	87.2	87.21	0.00%
14	101.3	101.3	-0.00%
15	113.3	113.3	0.00%
16	117	117	0.00%
17	122.7	122.7	0.00%
18	122.9	122.9	-0.00%
19	137.1	137.1	-0.00%
20	139.3	139.4	0.00%
21	143.6	143.6	0.00%
22	163.1	163	-0.00%
23	245.2	245.2	-0.00%
24	248.3	248.3	0.00%
25	258.9	258.9	-0.00%
26	288.4	288.5	0.00%
27	296.9	296.9	-0.00%
28	330.7	330.7	-0.00%
29	372.5	372.5	0.00%
30	440.4	440.4	-0.00%
31	444.2	444.2	0.00%

4.2 Modal Mass Participation Factors

The modal mass participation factors for the OpenSees model are compared to the participation factors listed in the NUREG report for excitations in X, Y, and Z directions in Tables 4.3, 4.4, and 4.5, respectively. Due to the identical eigenvalues between the SAP and OpenSees models, the modal mass participation factors also match, within round off error, for all three possible excitation directions.

The modal mass participation factors are computed using the `modalProperties` command in OpenSeesPy.

Table 4.3: Comparison of modal mass participation for X-direction from SAP V (un-numbered table on page A-11 of NUREG report) and OpenSeesPy

Mode	SAP V	OpenSees	Relative Diff
1	-2.34730e-02	-2.34726e-02	-0.00%
2	-5.56730e-01	5.56723e-01	-0.00%
3	-4.77190e-02	4.77186e-02	-0.00%
4	-9.95550e-03	-9.95519e-03	-0.00%
5	-1.53420e-01	1.53420e-01	0.00%
6	5.53640e-01	-5.53640e-01	-0.00%
7	-3.71190e-01	-3.71197e-01	0.00%
8	-4.02720e-01	4.02707e-01	-0.00%
9	5.59950e-01	5.59998e-01	0.01%
10	9.28280e-02	9.28255e-02	-0.00%
11	-1.43510e+00	-1.43514e+00	0.00%
12	4.29560e-01	4.29544e-01	-0.00%
13	-3.22980e-01	-3.22956e-01	-0.01%
14	9.70480e-02	9.70493e-02	0.00%
15	-1.07960e-01	1.07961e-01	0.00%
16	-4.22170e-01	4.22168e-01	-0.00%
17	-3.24490e-02	-3.24483e-02	-0.00%
18	-1.43300e-01	1.43301e-01	0.00%
19	-3.87580e-01	-3.87581e-01	0.00%
20	-3.67880e-03	-3.67829e-03	-0.01%
21	-6.91620e-02	-6.91625e-02	0.00%
22	1.64980e-01	-1.64985e-01	0.00%
23	1.27660e-01	1.27662e-01	0.00%
24	-2.40410e-02	2.40411e-02	0.00%
25	-2.01860e-02	-2.01865e-02	0.00%
26	4.79430e-01	-4.79432e-01	0.00%
27	-8.37610e-02	-8.37610e-02	-0.00%
28	-3.36210e-01	3.36214e-01	0.00%
29	-2.51270e-03	2.51273e-03	0.00%
30	4.53970e-02	4.53942e-02	-0.01%
31	-5.35240e-01	-5.35242e-01	0.00%

Table 4.4: Comparison of modal mass participation for Y-direction from SAP V (un-numbered table on page A-11 of NUREG report) and OpenSeesPy

Mode	**SAP V**	**OpenSees**	**Relative Diff**
1	2.76950e-01	2.76945e-01	-0.00%
2	9.02790e-02	-9.02791e-02	0.00%
3	-9.46820e-01	9.46820e-01	0.00%
4	-2.13510e-01	-2.13509e-01	-0.00%
5	-4.58270e-01	4.58265e-01	-0.00%
6	3.98130e-01	-3.98139e-01	0.00%
7	3.93340e-01	3.93344e-01	0.00%
8	1.19400e+00	-1.19404e+00	0.00%
9	1.81190e-01	1.81180e-01	-0.01%
10	-1.47030e-01	-1.47021e-01	-0.01%
11	-1.96530e-01	-1.96517e-01	-0.01%
12	-2.48240e-01	-2.48229e-01	-0.00%
13	-1.51960e-01	-1.51967e-01	0.00%
14	4.11570e-01	4.11566e-01	-0.00%
15	4.03710e-02	-4.03711e-02	0.00%
16	-4.02110e-02	4.02113e-02	0.00%
17	-2.82970e-01	-2.82968e-01	-0.00%
18	8.62540e-02	-8.62540e-02	0.00%
19	1.15860e-01	1.15855e-01	-0.00%
20	-9.87050e-01	-9.87053e-01	0.00%
21	8.08460e-02	8.08466e-02	0.00%
22	-1.87270e-02	1.87267e-02	-0.00%
23	7.39490e-01	7.39486e-01	-0.00%
24	-3.39160e-01	3.39161e-01	0.00%
25	3.32980e-01	3.32977e-01	-0.00%
26	-1.66650e-02	1.66644e-02	-0.00%
27	-2.65440e-01	-2.65436e-01	-0.00%
28	4.70510e-02	-4.70515e-02	0.00%
29	2.46140e-04	-2.46135e-04	-0.00%
30	1.73560e-03	1.73555e-03	-0.00%
31	-1.24300e-02	-1.24298e-02	-0.00%

As noted in Table 4.5, the 0.54% relative difference in modal mass participation factors in the Z-direction for mode 10 is due to round off errors as the magnitude of the actual mass participation factors is very low, on the order of 1e-4.

Table 4.5: Comparison of modal mass participation for Z-direction from SAP V (un-numbered table on page A-11 of NUREG report) and OpenSeesPy

Mode	**SAP V**	**OpenSees**	**Relative Diff**
1	3.54370e-02	3.54367e-02	-0.00%
2	-1.09260e-01	1.09261e-01	0.00%
3	-1.92030e-01	1.92027e-01	-0.00%
4	6.84190e-01	6.84182e-01	-0.00%
5	7.44230e-01	-7.44230e-01	-0.00%
6	-3.50220e-01	3.50222e-01	0.00%
7	4.59140e-01	4.59135e-01	-0.00%
8	-1.14660e-02	1.14606e-02	-0.05%
9	-7.07720e-02	-7.07638e-02	-0.01%
10	-2.74720e-04	-2.76204e-04	0.54%
11	-3.42710e-01	-3.42712e-01	0.00%
12	-4.57130e-01	-4.57134e-01	0.00%
13	-5.34360e-02	-5.34412e-02	0.01%
14	2.99440e-01	2.99436e-01	-0.00%
15	4.30200e-01	-4.30198e-01	-0.00%
16	2.90740e-01	-2.90737e-01	-0.00%
17	-2.11270e-01	-2.11272e-01	0.00%
18	-6.10270e-01	6.10268e-01	-0.00%
19	-5.37840e-02	-5.37836e-02	-0.00%
20	7.50350e-02	7.50352e-02	0.00%
21	1.18330e+00	1.18335e+00	0.00%
22	1.61000e+00	-1.61004e+00	0.00%
23	-2.91010e-02	-2.91005e-02	-0.00%
24	-6.47570e-03	6.47541e-03	-0.00%
25	-1.98970e-02	-1.98966e-02	-0.00%
26	-6.20620e-02	6.20608e-02	-0.00%
27	2.65150e-02	2.65144e-02	-0.00%
28	1.17050e-01	-1.17049e-01	-0.00%
29	-5.06360e-01	5.06356e-01	-0.00%
30	-6.23250e-01	-6.23244e-01	-0.00%
31	-6.29820e-02	-6.29786e-02	-0.01%

An additional calculation (not presented in the NUREG report) of the cumulative mass participation factor for each direction of excitation is shown in Table 4.6. For the 31 modes considered in the NUREG report, only 55.78% of the BM3 model mass participates in X-direction excitation. To achieve 90% mass participation, the "missing mass" from modes 32 and higher must be taken into account for modal superposition and response spectrum analysis. Simiarly, 62.72% and 85.78% of the system mass participates in excitations in the Y- and Z-directions.

Table 4.6: Mass participation factors (cumulative) for all directions of excitation based on OpenSeesPy model.

Mode	X**-Direction**	Y**-Direction**	Z**-Direction**
1	0.01%	0.92%	0.01%
2	3.71%	1.01%	0.16%
3	3.73%	11.71%	0.60%
4	3.73%	12.26%	6.19%
5	4.02%	14.77%	12.80%
6	7.67%	16.66%	14.26%
7	9.32%	18.50%	16.78%
8	11.26%	35.52%	16.78%
9	15.00%	35.92%	16.84%
10	15.10%	36.17%	16.84%
11	39.69%	36.64%	18.24%
12	41.89%	37.37%	20.74%
13	43.14%	37.65%	20.77%
14	43.25%	39.67%	21.84%
15	43.39%	39.69%	24.05%
16	45.52%	39.71%	25.06%
17	45.53%	40.66%	25.59%
18	45.77%	40.75%	30.04%
19	47.57%	40.91%	30.07%
20	47.57%	52.54%	30.14%
21	47.62%	52.62%	46.86%
22	47.95%	52.63%	77.80%
23	48.14%	59.15%	77.81%
24	48.15%	60.53%	77.81%
25	48.16%	61.85%	77.82%
26	50.90%	61.85%	77.86%
27	50.98%	62.69%	77.87%
28	52.33%	62.72%	78.03%
29	52.33%	62.72%	81.09%
30	52.36%	62.72%	85.73%
31	55.78%	62.72%	85.78%

4.3 Damping

As described in the NUREG report, the BM3 analysis used Rayleigh damping with 1% and 5% critical damping targeted to the fundamental frequency and an intermediate frequency of 11.5 Hz (72.3 rad/sec). The resulting 1% and 5% damping spectra for the BM3 model are shown in Figure 4.2 where the damping imposed on modes 23 and higher is over three times higher than the target damping ratio.

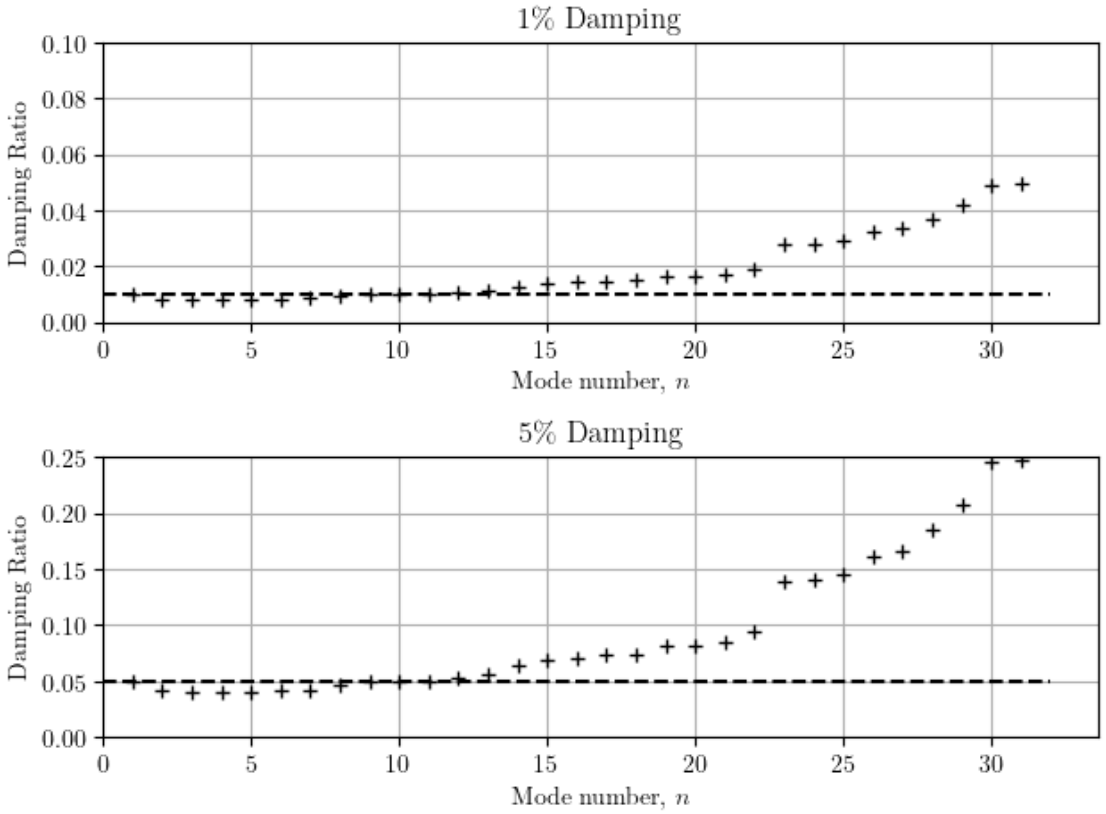

Figure 4.2: 1% and 5% damping spectra for BM3 pipe network model.

4.4 Input Ground Acceleration

The ground acceleration imposed as X-direction excitation on the BM3 model is shown in Figure 4.3. The digitization is 0.01 sec and the peak ground acceleration (PGA) is approximately 0.54g.

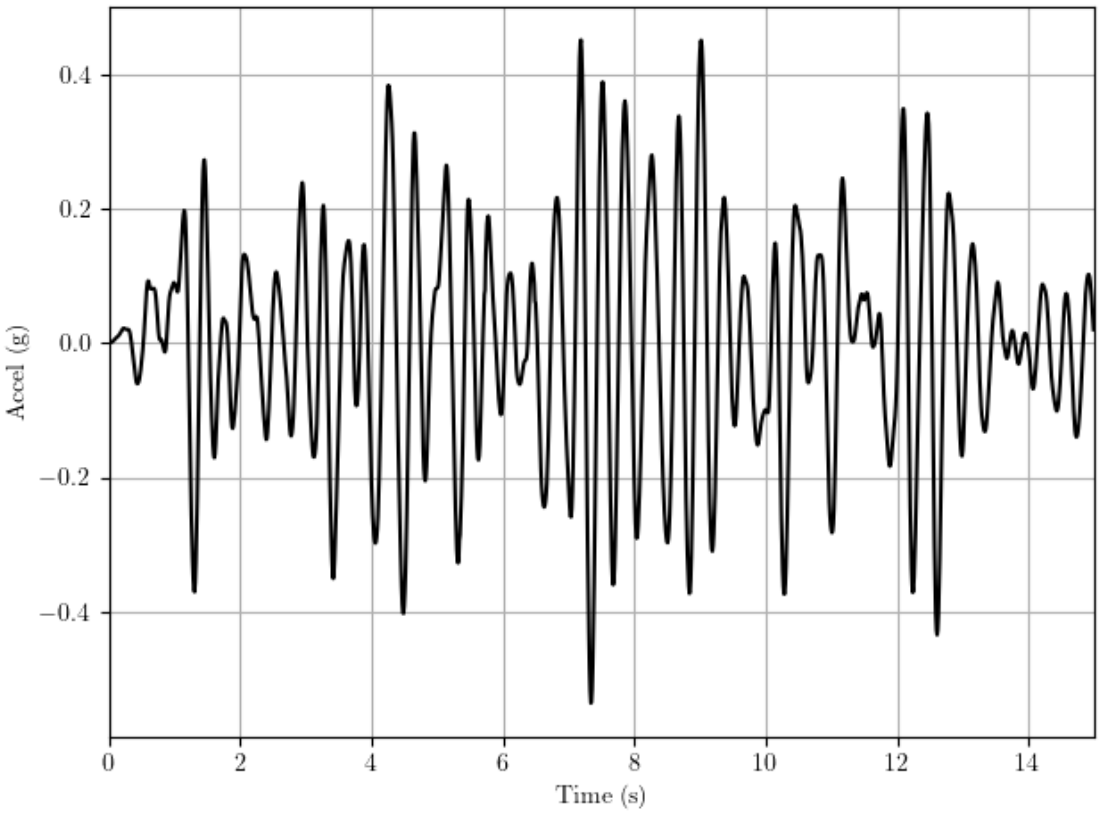

Figure 4.3: Input ground acceleration for dynamic analysis of BM3 pipe network model.

The acceleration response spectra for the input ground acceleration of Figure 4.3 are shown in Figure 4.4 for 1% and 5% damping. The zero period acceleration (ZPA) is equal to the 0.54g PGA and, as described in section 3.1 of the NUREG report, the ZPA is applied to modes whose natural frequency is higher than 16.5 Hz (103.7 rad/sec circular frequency).

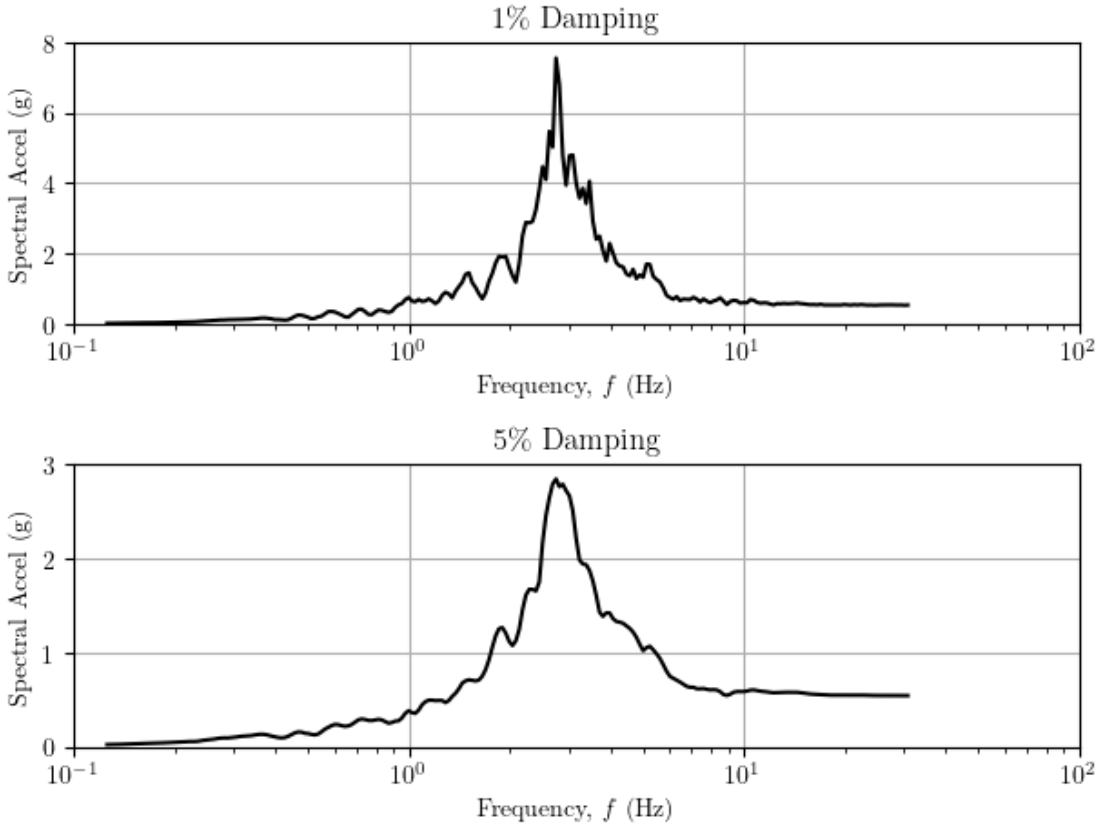

Figure 4.4: Input response spectra for dynamic analysis of BM3 pipe network model.

4.5 Static Analysis for Zero Period Acceleration

SAP V uses different mass distributions for static and dynamic analyses. For static analysis, e.g., for self-weight calculations, the mass of piping elements is assumed to be distributed along the element length (leading to distributed force under constant acceleration). On the other hand, for dynamic analysis, SAP V uses lumped nodal mass, assembled from element contributions.

Static analyses were performed in the NUREG report in order to ensure the mass distributions used by SAP V for static and dynamic analysis are sufficiently refined and give similar results for external reactions and internal bending moments. For each distribution of mass, a static analysis was performed in OpenSees by imposing a constant X-direction acceleration (equal to the 0.54g ZPA) to the BM3 model, leading to equivalent nodal forces for the dynamic case of lumped mass and distributed element loads for the static case of distributed mass.

4.5.1 Lumped Nodal Mass

Performing static analysis for the ZPA applied in the X-direction of the OpenSees model gives the fixed support reactions shown in Table 4.7. The reactions obtained from OpenSees are generally within 1% of the reactions listed in the NUREG report for the SAP V analysis.

Table 4.7: Comparison of peak support reactions obtained from SAP V (Table C-1 in NUREG report) and OpenSeesPy for static analysis at the ZPA using lumped mass (units = lb, inch)

Node	**Reaction**	**SAP V**	**OpenSees**	**Relative Diff**
1	FX	-46.21	-46.13	-0.18%
1	FY	0.66	0.66	-0.57%
1	FZ	0.26	0.26	1.72%
1	MX	10.53	10.51	-0.24%
1	MY	-329.25	-328.62	-0.19%
1	MZ	158.43	158.16	-0.17%
4	FX	-102.75	-102.56	-0.19%
4	FZ	-5.49	-5.48	-0.27%
7	FY	-0.01	-0.01	-38.17%
11	FY	-1.17	-1.17	0.18%
11	FZ	37.65	37.57	-0.20%
15	FX	-474.26	-473.37	-0.19%
17	FY	3.78	3.77	-0.17%
17	FZ	-35.17	-35.11	-0.18%
36	FY	8.92	8.90	-0.24%
36	FZ	31.68	31.63	-0.17%
38	FX	-767.29	-765.87	-0.19%
38	FY	-11.24	-11.22	-0.20%
38	FZ	-31.17	-31.11	-0.18%
38	MX	-189.06	-188.69	-0.20%
38	MY	-2202.83	-2198.79	-0.18%
38	MZ	804.58	802.99	-0.20%
23	FX	-304.11	-303.56	-0.18%
23	FY	-0.68	-0.68	0.61%
31	FX	-56.51	-56.41	-0.17%
31	FY	-0.25	-0.25	-0.61%
31	FZ	2.24	2.23	-0.42%
31	MX	219.27	218.72	-0.25%
31	MY	580.84	579.86	-0.17%
31	MZ	1702.48	1699.61	-0.17%

In addition to the reactions, the peak resultant member end moments are shown in Table 4.8 for the static analysis with the ZPA applied to the lumped nodal masses. The OpenSees results are consistently within 0.20% of the member end moments listed in the NUREG report for the SAP V analysis.

Table 4.8: Comparison of peak resultant end moments obtained from SAP V (Table C-2 in NUREG report) and OpenSeesPy for static analysis at the ZPA using lumped mass (units = lb,inch)

Note that the NUREG report lists the peak resultant moment at end J of each element.

Element	**SAP V**	**OpenSees**	**Relative Diff**
1	357.75	357.08	-0.19%
2	450.75	449.91	-0.19%
3	995.58	993.77	-0.18%
4	327.00	326.37	-0.19%
5	241.67	241.22	-0.19%
6	868.02	866.36	-0.19%
7	725.62	724.22	-0.19%
8	354.59	353.90	-0.19%
9	502.09	501.12	-0.19%
10	912.98	911.22	-0.19%
11	1617.18	1614.08	-0.19%
12	3951.97	3944.38	-0.19%
13	2956.60	2950.92	-0.19%
14	8613.31	8597.01	-0.19%
15	475.77	474.78	-0.21%
16	467.76	466.95	-0.17%
17	310.22	309.64	-0.19%
18	706.10	704.72	-0.20%
19	471.56	470.65	-0.19%
20	2028.91	2024.93	-0.20%
21	580.58	579.45	-0.20%
22	1971.49	1967.88	-0.18%
23	1167.59	1165.42	-0.19%
24	1123.54	1121.48	-0.18%
25	922.09	920.54	-0.17%
26	657.25	656.14	-0.17%
27	340.76	340.19	-0.17%
28	600.98	599.98	-0.17%
29	710.13	708.92	-0.17%
30	1812.15	1809.08	-0.17%
31	7523.23	7509.36	-0.18%
32	9107.41	9090.66	-0.18%
33	10884.84	10864.86	-0.18%
34	2199.42	2195.22	-0.19%
35	4815.86	4806.95	-0.18%
36	1247.94	1245.63	-0.19%
37	2352.78	2348.42	-0.19%

4.5.2 Distributed Element Mass

To account for distributed element mass, the mass density per unit length of each element in the OpenSees model is multiplied by the ZPA in order to obtain distributed member loads in the X-direction. Like the analysis based on lumped mass, Table 4.9 shows the reactions obtained from OpenSees for distributed element mass are generally within 1% of the SAP V analysis shown in the NUREG report. The relative difference for the FZ reaction of node 1 is very high because the computed values for this reaction are close to zero (less than 0.01 lb).

Table 4.9: Comparison of peak support reactions obtained from SAP V (Table C-1 in NUREG report) and OpenSeesPy for static analysis at the ZPA using distributed mass (units = lb, inch)

Node	**Reaction**	**SAP V**	**OpenSees**	**Relative Diff**
1	FX	-50.50	-50.45	-0.10%
1	FY	0.66	0.66	0.23%
1	FZ	0.01	-0.01	-211.82%
1	MX	32.80	32.77	-0.08%
1	MY	-478.00	-477.09	-0.19%
1	MZ	-823.00	-821.92	-0.13%
4	FX	-98.00	-97.78	-0.22%
4	FZ	-4.26	-4.25	-0.12%
7	FY	-0.85	-0.85	-0.47%
11	FY	-0.12	-0.12	3.06%
11	FZ	36.00	35.95	-0.13%
17	FY	3.84	3.83	-0.17%
17	FZ	-34.40	-34.35	-0.13%
36	FY	8.70	8.68	-0.20%
36	FZ	34.80	34.74	-0.17%
38	FX	-770.00	-768.74	-0.16%
38	FY	-11.20	-11.14	-0.51%
38	FZ	-35.60	-35.56	-0.13%
38	MX	-195.00	-194.62	-0.19%
38	MY	-2520.00	-2513.90	-0.24%
38	MZ	799.00	797.67	-0.17%
23	FX	-297.00	-296.01	-0.33%
23	FY	-0.15	-0.15	-2.83%
31	FX	-60.60	-60.52	-0.14%
31	FY	-0.92	-0.92	-0.11%
31	FZ	3.49	3.48	-0.27%
31	MX	344.00	343.62	-0.11%
31	MY	502.00	501.49	-0.10%
31	MZ	2200.00	2192.20	-0.35%

The resultant end moments obtained by static analysis at the ZPA using distributed element mass are shown in Table 4.10. Like the lumped mass static analysis, the differences between SAP

and OpenSees are consistently less than 0.2%.

Table 4.10: Comparison of peak resultant end moments obtained from SAP V (Table C-2 in NUREG report) and OpenSeesPy for static analysis at the ZPA using distributed mass (units = lb, inch)

Note that the NUREG report lists the peak resultant moment at end J of each element.

Element	**SAP V**	**OpenSees**	**Relative Diff**
1	961.37	959.59	-0.18%
2	808.88	807.38	-0.19%
3	1241.14	1238.84	-0.18%
4	526.13	525.15	-0.19%
5	303.25	302.69	-0.18%
6	627.91	626.74	-0.19%
7	486.36	485.46	-0.18%
8	179.01	178.74	-0.15%
9	498.37	497.44	-0.19%
10	836.15	834.60	-0.19%
11	1642.18	1639.13	-0.19%
12	3927.76	3920.47	-0.19%
13	2925.35	2919.92	-0.19%
14	8664.29	8648.22	-0.19%
15	503.56	502.62	-0.19%
16	445.32	444.50	-0.18%
17	302.07	301.51	-0.18%
18	755.46	754.06	-0.19%
19	519.70	518.74	-0.18%
20	2009.32	2005.60	-0.19%
21	524.32	523.35	-0.19%
22	1987.20	1983.54	-0.18%
23	1191.47	1189.28	-0.18%
24	1119.43	1117.37	-0.18%
25	788.22	786.76	-0.18%
26	536.09	535.10	-0.18%
27	257.71	257.24	-0.18%
28	502.43	501.50	-0.18%
29	578.43	577.36	-0.19%
30	2279.14	2274.93	-0.18%
31	7288.41	7274.98	-0.18%
32	8828.37	8812.12	-0.18%
33	10502.09	10482.75	-0.18%
34	2703.06	2698.07	-0.18%
35	5424.33	5414.34	-0.18%
36	1402.92	1400.34	-0.18%
37	2649.47	2644.59	-0.18%

4.6 Mode Superposition Time History Analysis

Although OpenSees does not perform modal superposition analysis within its core C++ computational framework, this type of analysis can be conducted via Python scripting, In this section, the modal superposition results presented in the NUREG report are compared to modal superposition conducted via OpenSeesPy scripts.

The NUREG report showed modal superposition results based on the first 31 modes of vibration of the BM3 model, both with and without the "missing mass" after 31 modes. To perform modal superposition, the mass of each node must be divided into participating and missing components for modal superposition with and without the missing mass effect. The procedure to compute missing mass is described in Appendix I of the NUREG report and summarized below. Further details on the missing mass approach, also referred to as static correction and mode acceleration superposition, can be found in Chapter 12 of [3].

For the i^{th} dynamic DOF in the model, the fraction of mass included in the mode superposition analysis is obtained via the sum

$$d_i = \sum_{n=1}^{N} \Gamma_{n,j} \phi_{n,i} \tag{4.1}$$

where N is the total number of modes includes in the mode superposition, $\Gamma_{n,j}$ is the participation factor for mode n in the j direction of excitation, and $\phi_{n,i}$ is the eigenvector component for DOF i in the n^{th} mode.

The "missing" mass not included for the i^{th} dynamic DOF in the mode superposition is then

$$e_i = d_i - \delta_{ij} \tag{4.2}$$

where δ_{ij} is the Kronecker delta, ensuring that missing mass is computed only for DOFs in the same direction as the excitation (direction j). The participating and missing mass components for each node of the BM3 model are summarized in Table 4.11.

Table 4.11: Participating and missing masses (up to and after 31 modes) in OpenSeesPy model (units = lb-sec^2/inch). (Compared to Table E-5 of the NUREG report)

Node	**Total**	**Participating** (d)	**Missing** (e)
1	0.017	-0.000	0.017
2	0.026	-0.000	0.026
3	0.212	0.001	0.211
4	0.227	0.000	0.227
5	0.031	0.024	0.007
6	0.165	0.166	-0.001
7	0.165	0.168	-0.003
8	0.092	0.093	-0.001
9	0.267	0.270	-0.003
10	0.275	0.277	-0.002
11	0.182	0.183	-0.001
12	0.174	0.174	0.000
13	0.092	0.091	0.000
14	0.059	0.053	0.006
15	0.101	0.008	0.093
16	0.059	0.054	0.004
17	0.105	0.106	-0.001
18	0.268	0.272	-0.004
19	0.180	0.183	-0.003
20	0.073	0.073	-0.000
21	0.207	0.170	0.037
22	0.088	0.066	0.022
23	0.043	0.038	0.005
24	0.052	0.052	-0.001
25	0.197	0.202	-0.005
26	0.178	0.190	-0.011
27	0.048	0.053	-0.005
28	0.063	0.072	-0.009
29	0.048	0.052	-0.003
30	0.175	0.165	0.010
31	0.158	0.000	0.158
32	0.163	0.149	0.013
33	0.276	0.280	-0.004
34	0.780	0.882	-0.102
35	0.687	0.090	0.597
36	0.687	0.007	0.680
37	1.170	0.006	1.164
38	0.585	0.000	0.585

4.6.1 1% Damping

The peak support reactions obtained from modal superposition for 31 modes of the BM3 model, with and without missing mass, are shown in Table 4.12 for 1% damping. The reactions obtained from only 31 modes (no missing mass) agree well between the SAP V analysis and OpenSees; however, there are a few cases, e.g., FY and MZ of node 1 and FX of node 38, where the inclusion of missing mass leads to larger differences between the two softwares. There is no clear trend in these reactions where the missing mass has a significant effect on the reaction magnitude.

Table 4.12: Comparison of peak support reactions obtained from SAP V (Table E-1 in NUREG report) and OpenSeesPy for modal superposition with and without missing mass for 1% damping (units = lb, inch)

		Modal (31 modes)			**Modal (31 modes + MM)**		
Node	**Reaction**	**SAP V**	**OpenSees**	**Relative Diff**	**SAP V**	**OpenSees**	**Relative Diff**
1	FX	8.40	8.54	1.69%	43.71	43.83	0.28%
1	FY	10.14	10.22	0.77%	4.36	3.27	-25.07%
1	FZ	1.60	1.63	2.05%	1.60	1.63	2.06%
1	MX	49.98	54.42	8.89%	49.88	54.31	8.88%
1	MY	776.73	785.60	1.14%	776.40	785.38	1.16%
1	MZ	193.46	191.99	-0.76%	278.42	275.96	-0.88%
4	FX	68.75	69.98	1.80%	116.79	118.40	1.38%
4	FZ	19.55	20.79	6.32%	20.01	21.27	6.31%
7	FY	13.31	13.78	3.51%	13.27	13.74	3.53%
11	FY	13.31	13.62	2.30%	13.31	13.62	2.30%
11	FZ	81.14	82.75	1.98%	81.34	82.95	1.97%
15	FX	713.32	724.24	1.53%	731.47	742.35	1.49%
17	FY	25.61	26.91	5.07%	25.60	26.91	5.11%
17	FZ	64.26	65.46	1.87%	65.36	66.61	1.91%
36	FY	46.31	47.92	3.48%	46.69	49.03	5.02%
36	FZ	48.85	48.90	0.10%	42.12	41.73	-0.93%
38	FX	128.79	129.42	0.49%	732.18	742.00	1.34%
38	FY	43.52	43.75	0.52%	43.44	43.68	0.54%
38	FZ	31.40	31.20	-0.63%	29.95	29.71	-0.79%
38	MX	720.04	741.43	2.97%	719.05	740.42	2.97%
38	MY	2142.00	2130.12	-0.55%	2084.97	2071.83	-0.63%
38	MZ	3088.90	3104.14	0.49%	3085.87	3101.28	0.50%
23	FX	259.22	263.79	1.76%	259.59	264.20	1.77%
23	FY	26.04	25.99	-0.18%	26.08	26.03	-0.19%
31	FX	23.24	23.19	-0.21%	55.05	56.09	1.89%
31	FY	14.21	14.24	0.23%	14.17	14.21	0.27%
31	FZ	16.07	16.57	3.09%	16.08	16.57	3.06%
31	MX	1136.90	1152.39	1.36%	1137.30	1152.65	1.35%
31	MY	608.43	619.62	1.84%	612.38	623.78	1.86%
31	MZ	1767.90	1783.20	0.87%	1773.20	1788.74	0.88%

In addition to the reactions of the BM3 model, the peak resultant moments of the pipe elements obtained by modal superposition are shown in Table 4.13 for 1% damping. Contrary to the peak

reactions which showed some significant differences in results, whether missing mass is included in the modal analysis or not, the peak end moments obtained from OpenSees are consistently within 2% of the peak moments obtained from SAP V.

Table 4.13: Comparison of peak resultant end moments obtained from SAP V (Table E-2 in NUREG report) and OpenSeesPy for modal superposition with and without missing mass for 1% damping (units = lb, inch)

	Modal (31 modes)			Modal (31 modes + MM)		
Element	**SAP V**	**OpenSees**	**Relative Diff**	**SAP V**	**OpenSees**	**Relative Diff**
1	823.40	831.60	1.00%	790.95	798.33	0.93%
2	818.58	826.71	0.99%	836.77	845.55	1.05%
3	1412.22	1437.08	1.76%	1429.28	1454.78	1.78%
4	762.56	769.66	0.93%	763.87	771.06	0.94%
5	598.91	607.60	1.45%	597.98	606.62	1.44%
6	2134.36	2160.71	1.23%	2133.18	2159.64	1.24%
7	1876.38	1896.42	1.07%	1877.81	1897.97	1.07%
8	852.96	850.02	-0.34%	852.74	849.74	-0.35%
9	1415.46	1433.31	1.26%	1415.21	1433.09	1.26%
10	1945.32	1976.84	1.62%	1946.24	1977.71	1.62%
11	3826.15	3844.85	0.49%	3829.46	3848.32	0.49%
12	8440.47	8516.39	0.90%	8428.48	8504.16	0.90%
13	6741.68	6799.06	0.85%	6741.03	6798.43	0.85%
14	13241.93	13430.56	1.42%	13219.91	13407.91	1.42%
15	2290.84	2317.97	1.18%	2293.75	2320.83	1.18%
16	1698.69	1702.93	0.25%	1696.61	1700.82	0.25%
17	2455.47	2501.56	1.88%	2455.62	2501.69	1.88%
18	2360.13	2392.80	1.38%	2363.76	2396.45	1.38%
19	1623.90	1654.64	1.89%	1625.77	1656.47	1.89%
20	7539.21	7595.37	0.74%	7544.81	7601.15	0.75%
21	1595.61	1601.11	0.34%	1590.16	1595.53	0.34%
22	2042.84	2043.92	0.05%	2046.41	2047.50	0.05%
23	1800.75	1802.39	0.09%	1807.75	1809.24	0.08%
24	1522.11	1523.09	0.06%	1518.31	1519.31	0.07%
25	926.28	926.01	-0.03%	922.51	922.32	-0.02%
26	665.57	661.82	-0.56%	677.35	673.87	-0.51%
27	399.00	396.23	-0.69%	390.71	388.14	-0.66%
28	742.39	741.99	-0.05%	737.42	737.05	-0.05%
29	824.73	823.28	-0.18%	830.76	829.20	-0.19%
30	1988.96	2034.38	2.28%	1994.56	2040.11	2.28%
31	7437.70	7442.66	0.07%	7428.79	7433.78	0.07%
32	8931.45	8932.76	0.01%	8785.32	8790.34	0.06%
33	11421.16	11422.27	0.01%	10970.06	10976.71	0.06%
34	6096.62	6159.75	1.04%	5993.82	6050.80	0.95%
35	6633.91	6674.74	0.62%	6788.22	6834.61	0.68%
36	1942.86	1981.54	1.99%	1874.84	1909.98	1.87%
37	3538.74	3568.95	0.85%	3501.06	3529.87	0.82%

4.6.2 5% Damping

The modal superposition analyses are repeated for 5% damping, with and without missing mass, giving the peak support reactions shown in Table 4.14 and peak resultant moments shown in Table 4.15. Like the case of 1% damping, the peak reactions obtained with SAP V and OpenSees agree well when not including missing mass; however, there are a couple of outliers, e.g., FY of node 1 and FZ of node 38, where the inclusion of missing mass shows more significant differences between the two softwares. With the additional damping (compared to modal superposition with 1% damping), the peak resultant moments of the pipe elements in the BM3 model are slightly improved, with OpenSees consistently within 3% of the SAP V results, as shown in Table 4.15.

Table 4.14: Comparison of peak support reactions obtained from SAP V (Table E-3 in NUREG report) and OpenSeesPy for modal superposition with and without missing mass for 5% damping (units = lb, inch)

		Modal (31 modes)			**Modal (31 modes + MM)**		
Node	**Reaction**	**SAP V**	**OpenSees**	**Relative Diff**	**SAP V**	**OpenSees**	**Relative Diff**
1	FX	7.87	7.90	0.44%	44.22	44.68	1.04%
1	FY	11.33	11.39	0.51%	3.86	2.07	-46.44%
1	FZ	0.97	1.00	2.64%	0.97	1.00	2.67%
1	MX	19.11	19.65	2.82%	18.89	19.43	2.88%
1	MY	695.11	699.06	0.57%	694.80	698.85	0.58%
1	MZ	156.85	157.40	0.35%	240.22	237.44	-1.16%
4	FX	65.32	65.83	0.79%	113.70	114.06	0.32%
4	FZ	13.38	13.40	0.17%	13.85	13.86	0.10%
7	FY	8.01	8.14	1.60%	7.95	8.16	2.58%
11	FY	7.13	7.24	1.56%	7.13	7.24	1.56%
11	FZ	71.69	71.93	0.33%	71.89	72.11	0.31%
15	FX	672.79	672.94	0.02%	690.97	690.53	-0.06%
17	FY	20.15	20.17	0.10%	20.14	20.17	0.15%
17	FZ	58.91	58.91	0.01%	60.05	60.01	-0.07%
36	FY	37.58	38.43	2.26%	38.70	39.52	2.11%
36	FZ	50.25	51.14	1.78%	42.33	42.69	0.84%
38	FX	136.14	136.21	0.05%	740.68	751.26	1.43%
38	FY	38.25	39.13	2.31%	38.18	39.07	2.32%
38	FZ	31.43	32.04	1.94%	29.85	30.36	1.70%
38	MX	466.39	473.64	1.55%	465.42	472.61	1.55%
38	MY	2143.30	2182.92	1.85%	2080.83	2117.05	1.74%
38	MZ	2715.60	2779.16	2.34%	2713.20	2776.52	2.33%
23	FX	270.09	270.37	0.10%	270.50	270.81	0.11%
23	FY	10.54	11.51	9.18%	10.58	11.50	8.65%
31	FX	22.57	22.64	0.29%	54.46	55.55	2.00%
31	FY	9.62	9.71	0.88%	9.76	9.81	0.54%
31	FZ	8.66	8.68	0.19%	8.66	8.69	0.30%
31	MX	559.28	573.74	2.59%	560.28	574.26	2.49%
31	MY	578.29	586.42	1.41%	582.28	590.59	1.43%
31	MZ	1679.80	1694.79	0.89%	1685.20	1700.33	0.90%

Table 4.15: Comparison of peak resultant end moments obtained from SAP V (Table E-4 in NUREG report) and OpenSeesPy for modal superposition with and without missing mass for 5% damping (units = lb, inch)

	Modal (31 modes)			Modal (31 modes + MM)		
Element	**SAP V**	**OpenSees**	**Relative Diff**	**SAP V**	**OpenSees**	**Relative Diff**
1	745.97	748.50	0.34%	713.05	717.00	0.55%
2	746.03	748.03	0.27%	765.02	766.35	0.17%
3	1306.36	1306.90	0.04%	1323.65	1324.39	0.06%
4	683.45	687.94	0.66%	684.42	688.90	0.65%
5	529.22	532.93	0.70%	528.66	532.40	0.71%
6	1894.42	1908.39	0.74%	1893.29	1907.41	0.75%
7	1663.22	1679.15	0.96%	1664.64	1680.59	0.96%
8	765.19	776.04	1.42%	764.93	775.74	1.41%
9	1320.17	1345.48	1.92%	1319.86	1345.26	1.92%
10	1713.20	1717.57	0.26%	1714.12	1718.39	0.25%
11	3504.53	3532.33	0.79%	3507.84	3535.60	0.79%
12	7662.41	7692.32	0.39%	7650.43	7680.72	0.40%
13	6075.86	6112.33	0.60%	6075.21	6111.74	0.60%
14	12509.76	12516.24	0.05%	12487.74	12494.17	0.05%
15	2027.62	2031.74	0.20%	2030.00	2034.23	0.21%
16	1057.72	1055.89	-0.17%	1057.35	1055.52	-0.17%
17	1496.87	1510.93	0.94%	1495.69	1509.81	0.94%
18	2023.46	2067.40	2.17%	2027.05	2070.75	2.16%
19	1368.94	1403.44	2.52%	1370.50	1405.10	2.52%
20	6607.12	6768.68	2.45%	6612.74	6773.97	2.44%
21	1340.38	1370.23	2.23%	1337.38	1368.63	2.34%
22	1789.34	1820.12	1.72%	1803.08	1835.55	1.80%
23	1339.89	1344.29	0.33%	1352.91	1355.53	0.19%
24	1236.93	1236.68	-0.02%	1229.48	1229.14	-0.03%
25	962.11	966.96	0.50%	958.32	963.22	0.51%
26	677.97	681.35	0.50%	689.97	693.49	0.51%
27	328.88	328.81	-0.02%	322.88	322.81	-0.02%
28	630.00	640.35	1.64%	624.60	634.62	1.60%
29	731.43	744.36	1.77%	737.73	751.23	1.83%
30	1777.89	1799.91	1.24%	1784.26	1806.39	1.24%
31	7221.12	7350.75	1.80%	7194.98	7320.79	1.75%
32	8935.01	9039.34	1.17%	8768.03	8878.40	1.26%
33	11395.76	11546.39	1.32%	10912.71	11072.89	1.47%
34	5486.76	5556.18	1.27%	5338.54	5440.15	1.90%
35	6167.02	6171.45	0.07%	6348.71	6348.32	-0.01%
36	1835.19	1835.34	0.01%	1755.84	1755.72	-0.01%
37	3308.12	3307.71	-0.01%	3263.83	3264.35	0.02%

4.7 Direct Integration Time History Analysis

Direct integration of the governing dynamic equilibrium equations accounts for all modes of response. OpenSees performs direct integration within its C++ computational core. Using 1% and 5% Rayleigh damping and the input ground acceleration record described previously in this chapter, dynamic analysis is performed in OpenSees and compared to the SAP V results shown in the NUREG report. For all OpenSees analyses, the Wilson-Theta time integrator is used with a 0.001 sec time step.

4.7.1 1% Damping

The peak reactions of the BM3 model, obtained by direct integration with 1% Rayleigh damping, are shown in Table 4.16. In addition to peak values, the times at which the peak occurred are also shown in the table. The times of peak occurrence match very well (within 0.01 sec) for the SAP V and OpenSees analyses. In addition, the magnitudes of the peak reaction forces are generally within 5%, save for the MX reaction of nodes 1 and 38.

The times of occurrence for peak end moments of the pipe elements in the BM3 model also agree well between SAP V and OpenSees as shown in Table 4.17. In addition, the magnitudes of the peak moments are generally within 5% for the two softwares.

4.7.2 5% Damping

The direct integration analysis is repeated for 5% Rayleigh damping with peak reactions and end moments shown in Tables 4.18 and 4.19, respectively. The times of peak occurrence agree for nearly all response quantities and the differences between OpenSees and SAP V are generally less compared to the direct integration analysis with 1% damping.

Table 4.16: Comparison of peak support reactions obtained from SAP V (Table E-1 in NUREG report) and OpenSeesPy for direct integration with 1% damping (units = lb, inch)

		SAP V		**OpenSees**		
Node	**Reaction**	**Peak**	at **Time** (s)	**Peak**	at **Time** (s)	**Relative Diff**
1	FX	43.63	7.35	43.83	7.34	0.46%
1	FY	3.35	4.69	3.29	4.69	-1.82%
1	FZ	1.59	7.35	1.65	1.59	4.02%
1	MX	45.14	6.68	54.80	6.68	21.41%
1	MY	778.76	7.35	789.47	7.35	1.38%
1	MZ	279.55	7.35	276.14	7.35	-1.22%
4	FX	117.78	7.35	118.63	7.35	0.72%
4	FZ	21.03	7.35	21.55	7.35	2.45%
7	FY	13.78	12.89	14.03	12.89	1.85%
11	FY	13.74	12.73	14.21	12.73	3.40%
11	FZ	82.49	7.35	83.57	7.35	1.31%
15	FX	740.29	7.35	746.12	7.35	0.79%
17	FY	27.45	11.01	28.20	11.01	2.73%
17	FZ	66.32	7.35	67.27	7.35	1.43%
36	FY	47.26	4.80	48.99	4.66	3.66%
36	FZ	41.80	4.46	43.49	4.46	4.05%
38	FX	736.41	7.35	743.06	7.34	0.90%
38	FY	42.51	7.36	43.46	7.36	2.24%
38	FZ	29.49	4.48	30.08	4.48	2.00%
38	MX	719.65	7.33	767.97	7.33	6.71%
38	MY	2055.80	4.48	2096.91	4.48	2.00%
38	MZ	3018.90	7.36	3087.12	7.36	2.26%
23	FX	265.71	4.47	268.59	4.47	1.08%
23	FY	24.60	7.38	26.81	7.38	8.99%
31	FX	55.78	7.35	56.10	7.35	0.57%
31	FY	14.20	10.56	14.76	10.56	3.92%
31	FZ	16.90	11.83	17.77	11.83	5.14%
31	MX	1173.80	11.84	1242.58	11.84	5.86%
31	MY	620.26	7.35	625.57	7.35	0.86%
31	MZ	1776.60	7.35	1793.93	7.35	0.98%

Table 4.17: Comparison of peak resultant end moments obtained from SAP V (Table E-2 in NUREG report) and OpenSeesPy for direct integration with 1% damping (units = lb, inch).

Note that the NUREG report lists the peak resultant moment at end J of each element.

	SAP V		**OpenSees**		
Element	**Peak**	at **Time** (s)	**Peak**	at **Time** (s)	**Relative Diff**
1	791.02	7.35	801.25	7.35	1.29%
2	838.40	7.35	848.73	7.35	1.23%
3	1441.59	7.35	1457.03	7.35	1.07%
4	764.19	7.35	774.42	7.35	1.34%
5	602.54	7.35	612.12	7.35	1.59%
6	2141.09	7.35	2170.12	7.35	1.36%
7	1880.06	7.35	1906.39	7.35	1.40%
8	832.43	4.65	854.48	4.65	2.65%
9	1438.67	4.66	1460.40	4.66	1.51%
10	1967.00	7.35	1993.49	7.35	1.35%
11	3804.39	7.35	3852.53	7.35	1.27%
12	8437.39	7.35	8541.44	7.35	1.23%
13	6738.07	7.35	6827.24	7.35	1.32%
14	13373.34	7.35	13471.74	7.35	0.74%
15	2364.57	4.67	2424.28	4.67	2.53%
16	1697.84	10.56	1770.47	10.56	4.28%
17	2492.35	10.66	2623.57	10.66	5.27%
18	2349.31	7.35	2409.71	7.35	2.57%
19	1623.68	7.35	1670.55	7.35	2.89%
20	7484.45	7.35	7620.23	7.35	1.81%
21	1564.96	7.35	1603.04	7.35	2.43%
22	2036.58	10.56	2103.87	10.56	3.30%
23	1802.73	10.56	1860.52	10.56	3.21%
24	1514.11	10.56	1561.03	10.56	3.10%
25	915.35	7.34	912.09	7.35	-0.36%
26	674.46	7.34	669.44	7.34	-0.74%
27	387.38	7.34	399.28	7.34	3.07%
28	734.60	7.34	748.28	7.34	1.86%
29	825.51	7.35	836.56	7.34	1.34%
30	2042.35	7.35	2068.68	7.35	1.29%
31	7377.43	10.56	7613.48	10.56	3.20%
32	8703.23	7.35	8779.45	7.35	0.88%
33	10866.98	7.34	10963.24	7.35	0.89%
34	5966.82	7.35	6065.88	7.35	1.66%
35	6757.74	7.35	6844.05	7.35	1.28%
36	1892.65	7.35	1919.86	7.35	1.44%
37	3487.86	7.35	3531.12	7.35	1.24%

Table 4.18: Comparison of peak support reactions obtained from SAP V (Table E-3 in NUREG report) and OpenSeesPy for direct integration with 5% damping (units = lb, inch)

		SAP V		**OpenSees**		
Node	**Reaction**	**Peak**	at **Time** (s)	**Peak**	at **Time** (s)	**Relative Diff**
1	FX	44.19	7.35	44.56	7.34	0.84%
1	FY	2.24	7.39	2.13	7.94	-4.70%
1	FZ	1.02	7.49	1.04	7.49	2.21%
1	MX	18.84	4.51	19.70	4.51	4.54%
1	MY	703.87	7.36	716.46	7.36	1.79%
1	MZ	239.67	7.37	240.14	7.36	0.19%
4	FX	113.82	7.35	114.76	7.35	0.82%
4	FZ	14.07	7.36	14.28	7.36	1.47%
7	FY	8.26	7.61	8.38	7.61	1.40%
11	FY	7.54	12.73	7.74	12.73	2.63%
11	FZ	72.60	7.36	73.74	7.36	1.57%
15	FX	692.19	7.36	701.05	7.36	1.28%
17	FY	20.26	7.38	20.53	7.38	1.35%
17	FZ	60.27	7.36	61.15	7.36	1.46%
36	FY	39.84	7.37	40.79	7.37	2.37%
36	FZ	41.88	12.61	43.07	12.61	2.83%
38	FX	744.53	7.35	751.01	7.34	0.87%
38	FY	39.69	7.37	40.27	7.37	1.46%
38	FZ	29.61	7.19	30.39	7.19	2.62%
38	MX	481.87	7.49	493.00	7.49	2.31%
38	MY	2065.30	7.19	2118.19	7.19	2.56%
38	MZ	2820.50	7.37	2861.65	7.37	1.46%
23	FX	268.35	12.60	271.92	12.60	1.33%
23	FY	10.97	6.57	12.46	6.57	13.56%
31	FX	55.10	7.35	55.59	7.34	0.88%
31	FY	10.16	7.50	10.33	7.50	1.64%
31	FZ	9.02	7.28	9.35	7.28	3.71%
31	MX	598.88	7.29	626.99	7.28	4.69%
31	MY	586.45	7.35	594.17	7.35	1.32%
31	MZ	1685.60	7.35	1707.99	7.35	1.33%

Table 4.19: Comparison of peak resultant end moments obtained from SAP V (Table E-4 in NUREG report) and OpenSeesPy for direct integration with 5% damping (units = lb, inch).

Note that the NUREG report lists the peak resultant moment at end J of each element.

	SAP V		**OpenSees**		
Element	**Peak**	at **Time** (s)	**Peak**	at **Time** (s)	**Relative Diff**
1	721.44	7.36	733.86	7.36	1.72%
2	772.40	7.36	782.92	7.36	1.36%
3	1326.79	7.36	1341.56	7.36	1.11%
4	693.18	7.36	706.14	7.36	1.87%
5	538.01	7.37	548.67	7.36	1.98%
6	1919.87	7.37	1956.72	7.36	1.92%
7	1695.52	7.37	1725.56	7.37	1.77%
8	781.15	7.37	792.26	7.37	1.42%
9	1362.63	7.37	1382.61	7.37	1.47%
10	1730.62	7.36	1756.43	7.36	1.49%
11	3557.59	7.37	3623.97	7.36	1.87%
12	7733.23	7.36	7858.83	7.36	1.62%
13	6149.10	7.36	6261.28	7.36	1.82%
14	12525.94	7.36	12680.26	7.36	1.23%
15	2061.56	7.37	2098.94	7.37	1.81%
16	1032.69	7.36	1066.54	1.72	3.28%
17	1523.29	7.37	1553.36	7.37	1.97%
18	2107.67	7.37	2140.85	7.37	1.57%
19	1433.54	7.37	1457.10	7.37	1.64%
20	6886.72	7.37	6985.92	7.37	1.44%
21	1397.33	7.37	1418.44	7.37	1.51%
22	1822.39	7.35	1848.64	7.35	1.44%
23	1368.99	7.36	1393.16	7.36	1.77%
24	1232.76	7.36	1253.01	7.36	1.64%
25	952.48	7.34	961.23	7.35	0.92%
26	687.08	7.34	692.67	7.35	0.81%
27	320.59	12.60	325.32	12.60	1.48%
28	635.75	7.35	644.39	7.35	1.36%
29	749.77	7.35	759.11	7.35	1.25%
30	1798.77	7.35	1821.51	7.35	1.26%
31	7240.74	7.35	7329.53	7.35	1.23%
32	8747.80	7.35	8858.30	7.35	1.26%
33	10913.38	7.35	11057.21	7.35	1.32%
34	5519.24	7.37	5597.55	7.37	1.42%
35	6378.37	7.36	6461.70	7.36	1.31%
36	1763.67	7.36	1786.19	7.36	1.28%
37	3278.70	7.36	3323.40	7.36	1.36%

4.8 Comparison of Direct Integration with Modal Superposition

A final comparison of SAP and OpenSees analysis shows the difference between direct integration response and the response obtained by modal superposition including the missing mass effect. With the missing mass effect, the modal superposition response should be the same as the response obtained by direct integration.

Unlike the previous comparisons, which quantify the differences between SAP and OpenSees analysis results, this comparison is meant to show the differences within each software–comparing direction integration and modal superposition from SAP and separately the results of the same analyses obtained from OpenSees.

4.8.1 1% Damping

The comparisons of direct integration and modal superposition for 1% damping are shown in Tables 4.20 and 4.21 for reactions and resultant end moments, respectively. Despite a few spurious cases, both SAP and OpenSees are self-consistent with differences between direct integration and modal superposition under 3%.

For each software, the primary source of differences between direct integration and modal superposition is the damping model. Rayleigh damping, where the target damping ratio is achieved in only two modes, is used for direct integration, while each mode uses the target damping ratio in modal superposition.

Table 4.20: Comparison of peak support reactions obtained from SAP V and OpenSeesPy for direct integration and modal superposition with 1% damping (units = lb, inch)

		SAP V			**OpenSees**		
Node	**Reaction**	**Direct**	**Modal+MM**	**Relative Diff**	**Direct**	**Modal+MM**	**Relative Diff**
1	FX	43.63	43.71	0.18%	43.83	43.83	0.00%
1	FY	3.35	4.36	30.15%	3.29	3.27	-0.67%
1	FZ	1.59	1.60	0.63%	1.65	1.63	-1.27%
1	MX	45.14	49.88	10.50%	54.80	54.31	-0.90%
1	MY	778.76	776.40	-0.30%	789.47	785.38	-0.52%
1	MZ	279.55	278.42	-0.40%	276.14	275.96	-0.06%
4	FX	117.78	116.79	-0.84%	118.63	118.40	-0.20%
4	FZ	21.03	20.01	-4.85%	21.55	21.27	-1.27%
7	FY	13.78	13.27	-3.70%	14.03	13.74	-2.11%
11	FY	13.74	13.31	-3.13%	14.21	13.62	-4.16%
11	FZ	82.49	81.34	-1.39%	83.57	82.95	-0.75%
15	FX	740.29	731.47	-1.19%	746.12	742.35	-0.50%
17	FY	27.45	25.60	-6.74%	28.20	26.91	-4.57%
17	FZ	66.32	65.36	-1.45%	67.27	66.61	-0.98%
36	FY	47.26	46.69	-1.21%	48.99	49.03	0.09%
36	FZ	41.80	42.12	0.77%	43.49	41.73	-4.06%
38	FX	736.41	732.18	-0.57%	743.06	742.00	-0.14%
38	FY	42.51	43.44	2.19%	43.46	43.68	0.49%
38	FZ	29.49	29.95	1.56%	30.08	29.71	-1.22%
38	MX	719.65	719.05	-0.08%	767.97	740.42	-3.59%
38	MY	2055.80	2084.97	1.42%	2096.91	2071.83	-1.20%
38	MZ	3018.90	3085.87	2.22%	3087.12	3101.28	0.46%
23	FX	265.71	259.59	-2.30%	268.59	264.20	-1.64%
23	FY	24.60	26.08	6.02%	26.81	26.03	-2.91%
31	FX	55.78	55.05	-1.31%	56.10	56.09	-0.02%
31	FY	14.20	14.17	-0.21%	14.76	14.21	-3.71%
31	FZ	16.90	16.08	-4.85%	17.77	16.57	-6.74%
31	MX	1173.80	1137.30	-3.11%	1242.58	1152.65	-7.24%
31	MY	620.26	612.38	-1.27%	625.57	623.78	-0.29%
31	MZ	1776.60	1773.20	-0.19%	1793.93	1788.74	-0.29%

Table 4.21: Comparison of peak resultant end moments obtained from SAP V and OpenSeesPy for direct integration and modal superposition with 1% damping (units = lb, inch)

	SAP V			OpenSees		
Element	**Direct**	**Modal+MM**	**Relative Diff**	**Direct**	**Modal+MM**	**Relative Diff**
1	791.02	790.95	-0.01%	801.25	798.33	-0.36%
2	838.40	836.77	-0.19%	848.73	845.55	-0.37%
3	1441.59	1429.28	-0.85%	1457.03	1454.78	-0.15%
4	764.19	763.87	-0.04%	774.42	771.06	-0.43%
5	602.54	597.98	-0.76%	612.12	606.62	-0.90%
6	2141.09	2133.18	-0.37%	2170.12	2159.64	-0.48%
7	1880.06	1877.81	-0.12%	1906.39	1897.97	-0.44%
8	832.43	852.74	2.44%	854.48	849.74	-0.55%
9	1438.67	1415.21	-1.63%	1460.40	1433.09	-1.87%
10	1967.00	1946.24	-1.06%	1993.49	1977.71	-0.79%
11	3804.39	3829.46	0.66%	3852.53	3848.32	-0.11%
12	8437.39	8428.48	-0.11%	8541.44	8504.16	-0.44%
13	6738.07	6741.03	0.04%	6827.24	6798.43	-0.42%
14	13373.34	13219.91	-1.15%	13471.74	13407.91	-0.47%
15	2364.57	2293.75	-3.00%	2424.28	2320.83	-4.27%
16	1697.84	1696.61	-0.07%	1770.47	1700.82	-3.93%
17	2492.35	2455.62	-1.47%	2623.57	2501.69	-4.65%
18	2349.31	2363.76	0.62%	2409.71	2396.45	-0.55%
19	1623.68	1625.77	0.13%	1670.55	1656.47	-0.84%
20	7484.45	7544.81	0.81%	7620.23	7601.15	-0.25%
21	1564.96	1590.16	1.61%	1603.04	1595.53	-0.47%
22	2036.58	2046.41	0.48%	2103.87	2047.50	-2.68%
23	1802.73	1807.75	0.28%	1860.52	1809.24	-2.76%
24	1514.11	1518.31	0.28%	1561.03	1519.31	-2.67%
25	915.35	922.51	0.78%	912.09	922.32	1.12%
26	674.46	677.35	0.43%	669.44	673.87	0.66%
27	387.38	390.71	0.86%	399.28	388.14	-2.79%
28	734.60	737.42	0.38%	748.28	737.05	-1.50%
29	825.51	830.76	0.64%	836.56	829.20	-0.88%
30	2042.35	1994.56	-2.34%	2068.68	2040.11	-1.38%
31	7377.43	7428.79	0.70%	7613.48	7433.78	-2.36%
32	8703.23	8785.32	0.94%	8779.45	8790.34	0.12%
33	10866.98	10970.06	0.95%	10963.24	10976.71	0.12%
34	5966.82	5993.82	0.45%	6065.88	6050.80	-0.25%
35	6757.74	6788.22	0.45%	6844.05	6834.61	-0.14%
36	1892.65	1874.84	-0.94%	1919.86	1909.98	-0.51%
37	3487.86	3501.06	0.38%	3531.12	3529.87	-0.04%

4.8.2 5% Damping

Tables 4.22 and 4.23 compare direct integration and modal superposition for reactions and resultant end moments, respectively, with 5% damping. Similar to the 1% damping case, there are spurious cases with noticeable differences, but generally, both SAP and OpenSees are self-consistent with differences between direct integration and modal superposition under 3%.

Table 4.22: Comparison of peak support reactions obtained from SAP V and OpenSeesPy for direct integration and modal superposition with 5% damping (units = lb, inch)

		SAP V			OpenSees		
Node	**Reaction**	**Direct**	**Modal+MM**	**Relative Diff**	**Direct**	**Modal+MM**	**Relative Diff**
1	FX	44.19	44.22	0.07%	44.56	44.68	0.26%
1	FY	2.24	3.86	72.32%	2.13	2.07	-3.16%
1	FZ	1.02	0.97	-4.90%	1.04	1.00	-4.47%
1	MX	18.84	18.89	0.27%	19.70	19.43	-1.32%
1	MY	703.87	694.80	-1.29%	716.46	698.85	-2.46%
1	MZ	239.67	240.22	0.23%	240.14	237.44	-1.12%
4	FX	113.82	113.70	-0.11%	114.76	114.06	-0.61%
4	FZ	14.07	13.85	-1.56%	14.28	13.86	-2.89%
7	FY	8.26	7.95	-3.75%	8.38	8.16	-2.63%
11	FY	7.54	7.13	-5.44%	7.74	7.24	-6.42%
11	FZ	72.60	71.89	-0.98%	73.74	72.11	-2.20%
15	FX	692.19	690.97	-0.18%	701.05	690.53	-1.50%
17	FY	20.26	20.14	-0.59%	20.53	20.17	-1.76%
17	FZ	60.27	60.05	-0.37%	61.15	60.01	-1.86%
36	FY	39.84	38.70	-2.86%	40.79	39.52	-3.11%
36	FZ	41.88	42.33	1.07%	43.07	42.69	-0.89%
38	FX	744.53	740.68	-0.52%	751.01	751.26	0.03%
38	FY	39.69	38.18	-3.80%	40.27	39.07	-2.98%
38	FZ	29.61	29.85	0.81%	30.39	30.36	-0.09%
38	MX	481.87	465.42	-3.41%	493.00	472.61	-4.13%
38	MY	2065.30	2080.83	0.75%	2118.19	2117.05	-0.05%
38	MZ	2820.50	2713.20	-3.80%	2861.65	2776.52	-2.97%
23	FX	268.35	270.50	0.80%	271.92	270.81	-0.41%
23	FY	10.97	10.58	-3.56%	12.46	11.50	-7.73%
31	FX	55.10	54.46	-1.16%	55.59	55.55	-0.07%
31	FY	10.16	9.76	-3.94%	10.33	9.81	-4.97%
31	FZ	9.02	8.66	-3.99%	9.35	8.69	-7.15%
31	MX	598.88	560.28	-6.45%	626.99	574.26	-8.41%
31	MY	586.45	582.28	-0.71%	594.17	590.59	-0.60%
31	MZ	1685.60	1685.20	-0.02%	1707.99	1700.33	-0.45%

Table 4.23: Comparison of peak resultant end moments obtained from SAP V and OpenSeesPy for direct integration and modal superposition with 5% damping (units = lb, inch)

	SAP V			OpenSees		
Element	**Direct**	**Modal+MM**	**Relative Diff**	**Direct**	**Modal+MM**	**Relative Diff**
1	721.44	713.05	-1.16%	733.86	717.00	-2.30%
2	772.40	765.02	-0.96%	782.92	766.35	-2.12%
3	1326.79	1323.65	-0.24%	1341.56	1324.39	-1.28%
4	693.18	684.42	-1.26%	706.14	688.90	-2.44%
5	538.01	528.66	-1.74%	548.67	532.40	-2.97%
6	1919.87	1893.29	-1.38%	1956.72	1907.41	-2.52%
7	1695.52	1664.64	-1.82%	1725.56	1680.59	-2.61%
8	781.15	764.93	-2.08%	792.26	775.74	-2.09%
9	1362.63	1319.86	-3.14%	1382.61	1345.26	-2.70%
10	1730.62	1714.12	-0.95%	1756.43	1718.39	-2.17%
11	3557.59	3507.84	-1.40%	3623.97	3535.60	-2.44%
12	7733.23	7650.43	-1.07%	7858.83	7680.72	-2.27%
13	6149.10	6075.21	-1.20%	6261.28	6111.74	-2.39%
14	12525.94	12487.74	-0.30%	12680.26	12494.17	-1.47%
15	2061.56	2030.00	-1.53%	2098.94	2034.23	-3.08%
16	1032.69	1057.35	2.39%	1066.54	1055.52	-1.03%
17	1523.29	1495.69	-1.81%	1553.36	1509.81	-2.80%
18	2107.67	2027.05	-3.83%	2140.85	2070.75	-3.27%
19	1433.54	1370.50	-4.40%	1457.10	1405.10	-3.57%
20	6886.72	6612.74	-3.98%	6985.92	6773.97	-3.03%
21	1397.33	1337.38	-4.29%	1418.44	1368.63	-3.51%
22	1822.39	1803.08	-1.06%	1848.64	1835.55	-0.71%
23	1368.99	1352.91	-1.17%	1393.16	1355.53	-2.70%
24	1232.76	1229.48	-0.27%	1253.01	1229.14	-1.90%
25	952.48	958.32	0.61%	961.23	963.22	0.21%
26	687.08	689.97	0.42%	692.67	693.49	0.12%
27	320.59	322.88	0.71%	325.32	322.81	-0.77%
28	635.75	624.60	-1.75%	644.39	634.62	-1.52%
29	749.77	737.73	-1.61%	759.11	751.23	-1.04%
30	1798.77	1784.26	-0.81%	1821.51	1806.39	-0.83%
31	7240.74	7194.98	-0.63%	7329.53	7320.79	-0.12%
32	8747.80	8768.03	0.23%	8858.30	8878.40	0.23%
33	10913.38	10912.71	-0.01%	11057.21	11072.89	0.14%
34	5519.24	5338.54	-3.27%	5597.55	5440.15	-2.81%
35	6378.37	6348.71	-0.47%	6461.70	6348.32	-1.75%
36	1763.67	1755.84	-0.44%	1786.19	1755.72	-1.71%
37	3278.70	3263.83	-0.45%	3323.40	3264.35	-1.78%

4.9 OpenSees Comparison of Modal Superposition with Direct Integration using Modal Damping

The prior analysis results for direct integration used Rayleigh damping (1% or 5%), which meets the target damping ratio in only two modes of vibration. As shown in the damping spectra of Figure 4.2, the damping ratios for high frequency modes are significantly higher than the target value, leading to discrepances between direct integration and modal superposition where the target damping ratio is used in *all* modes of vibrations, not just in two modes.

OpenSees allows users to specify modal damping ratios [10] for direct integration analysis so that the damping in each mode of vibration can be controlled. While this analysis option was not presented in the NUREG/CR-6645 report, results are shown in this section for OpenSees analysis comparing direct integration with modal damping to modal superposition with missing mass. This comparison serves as an additional check on the results obtained using the straight and curved piping elements in OpenSees.

For 1% damping, the maximum reactions and maximum element end moments are compared in Table 4.24 and 4.25. The analysis results are virtually identical with slight differences for some values and 0% difference for most values. Similarly excellent agreement is shown in Table 4.26 and 4.27 for 5% damping.

Table 4.24: Comparison of peak support reactions obtained from OpenSeesPy for direct integration with 1% modal damping and modal superposition with missing mass using 1% damping (units = lb, inch)

		OpenSees		
Node	**Reaction**	**Direct**	**Modal+MM**	**Relative Diff**
1	FX	43.86	43.83	-0.06%
1	FY	3.27	3.27	-0.13%
1	FZ	1.63	1.63	0.00%
1	MX	54.31	54.31	-0.00%
1	MY	785.38	785.38	0.00%
1	MZ	275.99	275.96	-0.01%
4	FX	118.40	118.40	-0.00%
4	FZ	21.27	21.27	-0.00%
7	FY	13.74	13.74	-0.00%
11	FY	13.62	13.62	-0.00%
11	FZ	82.95	82.95	-0.00%
15	FX	742.38	742.35	-0.00%
17	FY	26.91	26.91	0.00%
17	FZ	66.61	66.61	-0.00%
36	FY	49.01	49.03	0.04%
36	FZ	41.64	41.73	0.20%
38	FX	745.44	742.00	-0.46%
38	FY	43.68	43.68	-0.00%
38	FZ	29.75	29.71	-0.11%
38	MX	740.40	740.42	0.00%
38	MY	2073.08	2071.83	-0.06%
38	MZ	3101.29	3101.28	-0.00%
23	FX	264.19	264.20	0.00%
23	FY	26.03	26.03	-0.01%
31	FX	56.09	56.09	-0.00%
31	FY	14.21	14.21	0.00%
31	FZ	16.57	16.57	0.00%
31	MX	1152.64	1152.65	0.00%
31	MY	623.81	623.78	-0.01%
31	MZ	1788.73	1788.74	0.00%

Table 4.25: Comparison of peak resultant end moments obtained from OpenSeesPy for direct integration with 1% modal damping and modal superposition with missing mass using 1% damping (units = lb, inch)

	OpenSees		
Element	**Direct**	**Modal+MM**	**Relative Diff**
1	798.37	798.33	-0.01%
2	845.56	845.55	-0.00%
3	1454.81	1454.78	-0.00%
4	771.06	771.06	-0.00%
5	606.61	606.62	0.00%
6	2159.63	2159.64	0.00%
7	1897.96	1897.97	0.00%
8	849.74	849.74	0.00%
9	1433.09	1433.09	0.00%
10	1977.71	1977.71	-0.00%
11	3848.31	3848.32	0.00%
12	8504.17	8504.16	-0.00%
13	6798.43	6798.43	0.00%
14	13407.87	13407.91	0.00%
15	2320.83	2320.83	0.00%
16	1700.82	1700.82	0.00%
17	2501.69	2501.69	0.00%
18	2396.39	2396.45	0.00%
19	1656.46	1656.47	0.00%
20	7601.05	7601.15	0.00%
21	1595.61	1595.53	-0.01%
22	2047.46	2047.50	0.00%
23	1809.32	1809.24	-0.00%
24	1519.36	1519.31	-0.00%
25	922.34	922.32	-0.00%
26	673.78	673.87	0.01%
27	388.14	388.14	-0.00%
28	737.06	737.05	-0.00%
29	829.19	829.20	0.00%
30	2040.12	2040.11	-0.00%
31	7433.89	7433.78	-0.00%
32	8791.58	8790.34	-0.01%
33	10980.67	10976.71	-0.04%
34	6051.01	6050.80	-0.00%
35	6838.10	6834.61	-0.05%
36	1909.29	1909.98	0.04%
37	3529.38	3529.87	0.01%

Table 4.26: Comparison of peak support reactions obtained from OpenSeesPy for direct integration with 5% modal damping and modal superposition with missing mass using 5% damping (units = lb, inch)

		OpenSees		
Node	**Reaction**	**Direct**	**Modal+MM**	**Relative Diff**
1	FX	44.69	44.68	-0.02%
1	FY	2.07	2.07	-0.09%
1	FZ	1.00	1.00	0.00%
1	MX	19.43	19.43	0.01%
1	MY	698.85	698.85	-0.00%
1	MZ	237.52	237.44	-0.03%
4	FX	114.03	114.06	0.02%
4	FZ	13.86	13.86	0.00%
7	FY	8.15	8.16	0.01%
11	FY	7.24	7.24	0.00%
11	FZ	72.11	72.11	0.00%
15	FX	690.55	690.53	-0.00%
17	FY	20.17	20.17	0.00%
17	FZ	60.01	60.01	-0.00%
36	FY	39.50	39.52	0.05%
36	FZ	42.94	42.69	-0.60%
38	FX	754.94	751.26	-0.49%
38	FY	39.07	39.07	-0.00%
38	FZ	30.41	30.36	-0.15%
38	MX	472.64	472.61	-0.01%
38	MY	2118.81	2117.05	-0.08%
38	MZ	2776.54	2776.52	-0.00%
23	FX	270.81	270.81	0.00%
23	FY	11.49	11.50	0.00%
31	FX	55.55	55.55	-0.01%
31	FY	9.81	9.81	0.00%
31	FZ	8.69	8.69	-0.01%
31	MX	574.27	574.26	-0.00%
31	MY	590.58	590.59	0.00%
31	MZ	1700.30	1700.33	0.00%

Table 4.27: Comparison of peak resultant end moments obtained from OpenSeesPy for direct integration with 5% modal damping and modal superposition with missing mass using 5% damping (units = lb, inch)

	OpenSees		
Element	**Direct**	**Modal+MM**	**Relative Diff**
1	717.03	717.00	-0.01%
2	766.36	766.35	-0.00%
3	1324.40	1324.39	-0.00%
4	688.90	688.90	0.00%
5	532.41	532.40	-0.00%
6	1907.41	1907.41	-0.00%
7	1680.58	1680.59	0.00%
8	775.74	775.74	0.00%
9	1345.26	1345.26	0.00%
10	1718.39	1718.39	0.00%
11	3535.59	3535.60	0.00%
12	7680.73	7680.72	-0.00%
13	6111.73	6111.74	0.00%
14	12494.15	12494.17	0.00%
15	2034.23	2034.23	-0.00%
16	1055.52	1055.52	-0.00%
17	1509.80	1509.81	0.00%
18	2070.69	2070.75	0.00%
19	1405.10	1405.10	-0.00%
20	6773.98	6773.97	-0.00%
21	1368.63	1368.63	0.00%
22	1835.84	1835.55	-0.02%
23	1355.81	1355.53	-0.02%
24	1229.28	1229.14	-0.01%
25	963.17	963.22	0.01%
26	693.34	693.49	0.02%
27	322.79	322.81	0.00%
28	634.60	634.62	0.00%
29	751.23	751.23	-0.00%
30	1806.36	1806.39	0.00%
31	7320.66	7320.79	0.00%
32	8881.14	8878.40	-0.03%
33	11079.44	11072.89	-0.06%
34	5441.56	5440.15	-0.03%
35	6355.58	6348.32	-0.11%
36	1756.65	1755.72	-0.05%
37	3263.18	3264.35	0.04%

Chapter 5

Additional Examples

All the files listed below are appended to the report. The `.inp` files are inputs for SAP and can be run via

```
cat example.inp | ./sapv > example.out
```

This command will produce the output files with `.out` extensions.

The OpenSees `.py` files are run with Python directly.

```
python3 example.py
```

While the one and two element examples, e.g., "one straight pipe" or "two curved pipes", are straightforward to visualize, the examples of a pipe network (1, 2, 8, 9, 10, and 22) are based on the network shown in Figure 5.1. Note that the model is plotted with `opsvis` [6] with default axis orientation. In addition, for simplicity, the curved pipe elements are drawn as straight lines.

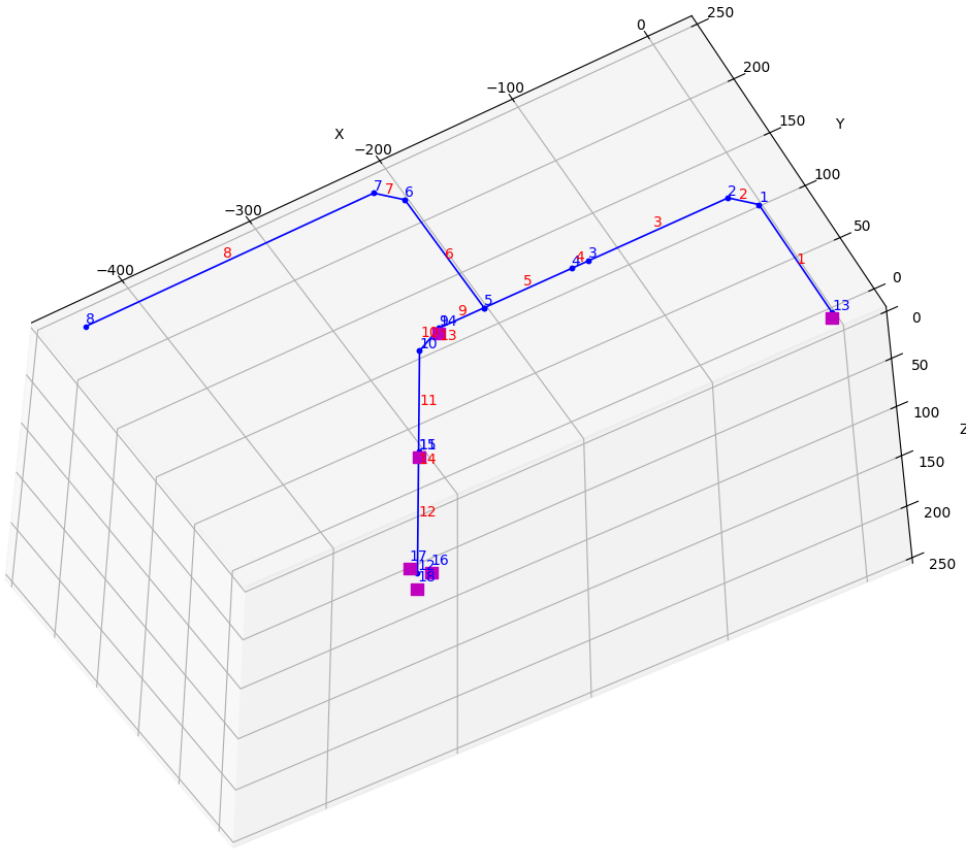

Figure 5.1: Element and node numbers for pipe network used in examples 1, 2, 8, 9, 10, and 22.

Example 1 Pipe network with point loads, shear deformation, thermal, and self-weight.

- example1.py
- example1.inp
- example1.out

Example 2 Pipe network with point loads and shear deformation

- example2.py
- example2.inp

- example2.out

Example 3-1 One straight pipe element with one end fixed and thermal loading.

- example31.py
- example3-1.inp
- example3-1.out

Example 3-2 One straight pipe element with one end fixed and internal pressure.

- example32.py
- example3-2.inp
- example3-2.out

Example 4 Two straight pipe elements eigenvalues

- example4.py
- example4.inp
- example4.out

Example 5 One straight pipe element with both ends pinned and thermal loading.

- example5.py
- example5.inp
- example5.out

Example 5-1 One straight pipe element with both ends pinned and self weight.

- example51.py
- example51.inp
- example51.out

Example 6 Pipe network with all elements straight and thermal loading.

- example6.py
- example6.inp
- example6.out

Example 7 One straight pipe element with one end fixed and another pinned and internal pressure.

- example7.py
- example7.inp
- example7.out

Example 8 Pipe network with all element straight and internal pressure

- example8.py
- example8.inp
- example8.out

Example 9 Pipe network with all element straight and both internal pressure and thermal loading.

- example9.py
- example9.inp
- example9.out

Example 10 Pipe network with all element straight and internal pressure, thermal loading, and shear deformation.

- example10.py
- example10.inp
- example10.out

Example 11 One curved pipe element with one end fixed and a point load.

- example11.py
- example11.inp
- example11.out

Example 12 Same as example 11 but the element bent in another direction.

- example12.py
- example12.inp
- example12.out

Example 13 One curved pipe element with one end fixed a point load and shear deformation

- example13.py
- example13.inp
- example13.out

Example 14 One curved pipe element with one end fixed and self-weight in y direction

- example14.py
- example14.inp
- example14.out

Example 15 One curved pipe element with one end fixed and point load in z direction.

- example15.py
- example15.inp
- example15.out

Example 16 One curved pipe element with one end fixed and self-weight in z direction

- example16.py
- example16.inp
- example16.out

Example 17 One curved pipe element with thermal loading.

- example17.py
- example17.inp
- example17.out

Example 18 One short curved pipe element with thermal loading.

- example18.py
- example18.inp
- example18.out

Example 19 One curved pipe element with internal pressure.

- example19.py
- example19.inp
- example19.out

Example 20 One curved pipe element with point load in x, y ,and z directions, self-weight in y direction, shear, thermal, and internal pressure.

- example20.py
- example20.inp
- example20.out

Example 21 Two straight elements with point load and shear deformation.

- example21.py
- example21.inp
- example21.out

Example 22 Pipe network with point loads.

- example22.py
- example22.inp
- example22.out

Example 23 One curved pipe element with point load in x, y ,and z directions, self-weight in y direction, shear, thermal, internal pressure, and a tangent intersection point.

- example23.py

- example23.inp
- example23.out

Example 24 Two curved pipe elements eigenvalue analysis

- example24.py
- example24.inp
- example24.out

Bibliography

[1] K.-J. Bathe, E. L. Wilson, and F. E. Peterson, *SAP IV: A Structural Analysis Program for Static and Dynamic Response of Linear Systems*. Earthquake Engineering Research Center (EERC), Report No. EERC-73-11, Berkeley, CA, 1973.

[2] Brookhaven National Laboratory (BNL), *Reevaluation of Regulatory Guidance on Modal Response Combination Methods for Seismic Response Spectrum Analysis*. Office of Nuclear Regulatory Research, Washington, D.C. Report No. NUREG/CR-6645, BNL-NUREG-52576, 1999.

[3] A. K. Chopra, *Dynamics of Structures: Theory and Applications to Earthquake Engineering*. 5th edition, Pearson, 2017.

[4] F. C. Filippou and G. L. Fenves, *Methods of Analysis for Earthquake-Resistant Structures*. in Earthquake Engineering: From Engineering Seismology to Performance-Based Engineering, CRC Press, Boca Raton, FL, 2004.

[5] A. S. Hall and R. W. Woodhead, *Frame Analysis*. Wiley, 1967.

[6] S. Kokot, *opsvis: OpenSeesPy Postprocessing and Visualization Module*. `https://opsvis.readthedocs.io`, Version 1.1.10, Website accessed September 2024.

[7] F. McKenna, M. H. Scott, and G. L. Fenves. "Nonlinear finite element analysis software architecture using object composition." *Journal of Computing in Civil Engineering*, 24(1):95-107, January 2010.

[8] National Information Service for Earthquake Engineering (NISEE), *Earthquake Engineering Software*, `https://nisee.berkeley.edu/elibrary/software.html`, PEER, Berkeley, CA, Website accessed October 2023.

[9] Open System for Earthquake Engineering Simulation (OpenSees), `https://opensees.berkeley.edu`, University of California, Berkeley, CA, 2000.

[10] E. Wilson and J. Penzien. "Evaluation of orthogonal damping matrices." *International Journal for Numerical Methods in Engineering*, 4(1):5–10, 1972.

[11] M. Zhu, F. McKenna, and M. H. Scott. "OpenSeesPy: Python library for the OpenSees finite element framework." *SoftwareX*, 7:6-11, June 2018.